

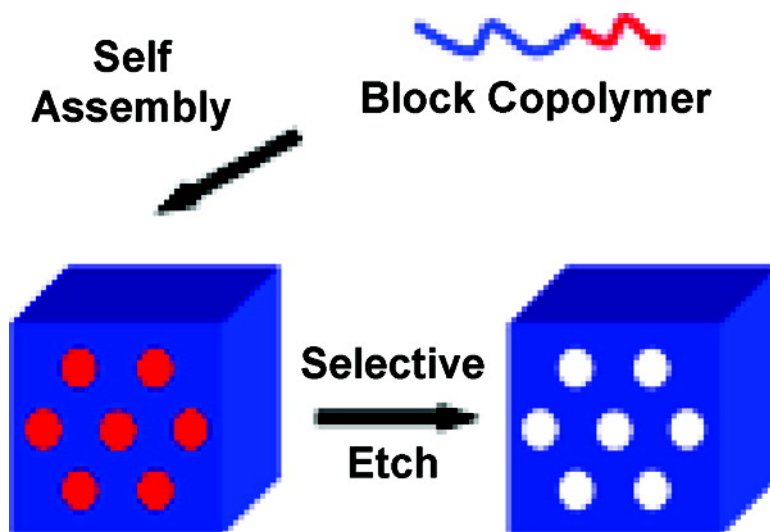
Review

Templating Nanoporous Polymers with Ordered Block Copolymers

David A. Olson, Liang Chen, and Marc A. Hillmyer

Chem. Mater., 2008, 20 (3), 869-890 • DOI: 10.1021/cm702239k • Publication Date (Web): 27 November 2007

Downloaded from <http://pubs.acs.org> on January 13, 2009



More About This Article

Additional resources and features associated with this article are available within the HTML version:

- Supporting Information
- Links to the 4 articles that cite this article, as of the time of this article download
- Access to high resolution figures
- Links to articles and content related to this article
- Copyright permission to reproduce figures and/or text from this article

[View the Full Text HTML](#)



ACS Publications

High quality. High impact.

Chemistry of Materials is published by the American Chemical Society. 1155 Sixteenth Street N.W., Washington, DC 20036

Templating Nanoporous Polymers with Ordered Block Copolymers[†]

David A. Olson, Liang Chen, and Marc A. Hillmyer*

Department of Chemistry, University of Minnesota, 207 Pleasant Street SE, Minneapolis, Minnesota 55455-0431

Received August 8, 2007. Revised Manuscript Received October 5, 2007

In the midst of this era of nanotechnology and shrinking device size, block copolymers have evolved from their use in traditional application areas (e.g., adhesives, additives, and elastomers) to enable the development of materials for new emerging and more advanced technologies. This review discusses the use of block copolymers to generate nanoporous polymers that can be used either directly, in applications such as membrane filtration, or subsequently as a template for the formation of other nanostructured materials. The work within describes published research from the beginning of 2005 to the present discussing nanoporous materials in the context of: (i) nanolithography and new alignment technologies, (ii) monoliths, (iii) new fabrication techniques, and (iv) membranes. A summary and perspective on the current direction of the stimulating area of block copolymer derived nanoporous materials concludes the review.

1. Introduction and Background

Block copolymers are hybrid macromolecules that have captured the attention of scientists and technologists over the past several decades. The “end-connecting” of distinct, incompatible polymeric segments into long chains leads to a predictable self-organization in which domains rich in one block are separated from domains rich in the other. Typical domain sizes are intimately tied to familiar macromolecular dimensions such as the radius of gyration. As such, the self-assembly of block copolymers naturally yields materials that are structured on the nanometer length scale. A now classic example is given by an AB diblock copolymer (i.e., one that contains a run of A monomers followed by a stretch of B monomers) with two-thirds A monomers and one-third B monomers. For most pairs of monomers at high enough overall molecular weight, long cylinders of B with nanoscopic (5–50 nm) diameters will organize on a hexagonal lattice in a continuous matrix of A. A few other ordered state morphologies that depend largely on the relative composition of A and B monomers can also form and are now well-established for a wide array of chemically distinct block copolymer molecules. The situation is more complex when a third block is in the mix. ABC terpolymers will also arrange themselves into nanostructured materials, but now with three distinct nanodomains. Of course, this opens up a much wider array of morphological possibilities, and there is a good deal of contemporary work (both experimental and theoretical) aimed at understanding the complexities associated with the self-assembly of ABC terpolymers. We point the interested reader to several books¹ and reviews² on the topic of block copolymer science for thorough expositions of the topic.

With the above discussion in mind, imagine a free-standing monolith or a supported thin film of an AB diblock copolymer with aligned nanoscopic B-rich cylinders in a

matrix of A. (The alignment of block copolymers in both the bulk and in thin films is a rich area of research,³ but beyond the scope of this article.) Now imagine “removing” all the B monomers to create voids where the cylinders were. Provided that the now-voided matrix of A does not collapse (i.e., it is mechanically robust enough to support such a pore structure), you will have generated a nanoporous version of polymer A. Figure 1 shows a visual schematic representation of this process. This example demonstrates how, by virtue of being connected to polyA, polyB can organize into nanodomains that in turn behave as templating or porogenic phases. This concept was introduced and demonstrated by Lee et al.⁴ two decades ago and has stimulated many other researchers to expand on, enhance, and develop this strategy. The primary enabling concept is that the minority component of the block copolymer is chemically, thermally, photochemically, or otherwise etchable, whereas the majority component is essentially “etch resistant.” Block copolymers that contain such sacrificial blocks, and their implementation, are the focus of this review. The “Templated Materials” that are typically generated by this protocol are nanoporous with pore dimensions generally ranging from a few to about 100 nm. These nanoporous materials are very useful, for example, for membrane separations or as high-surface-area supports. In fact, the nanoporous polymers generated in this way can themselves act as templates for the formation of other nanostructured materials.

We published a review in September 2005 that gave a historical perspective and summarized developments, advances, and new concepts in the area, through essentially the end of 2004.⁵ In the last two and a half years, at least 60 new publications describing some aspect of nanoporous materials from ordered block copolymer precursors have appeared and we attempt to organize and summarize these contributions in this review. Although not all the work we discuss utilizes a sacrificial block for the formation of nanoporosity, that is the general theme of the review.

[†] Part of the “Templated Materials Special Issue”.

* Corresponding author. E-mail: hillmyer@chem.umn.edu.

Much of the work has been done using block copolymer thin films, given their utility in lithographic or pattern transfer processes. This area of research has its origins in a seminal paper by Park et al. published in 1997.⁶ Section 2 following this introduction deals with the use of nanoporous materials derived from block copolymers in nanolithographic applications and is subdivided into a section focused generally on generation and applications of templates and a section that emphasizes so-called directed assembly techniques. In section 3, we discuss macroscopic or monolithic nanoporous polymers from ordered block copolymers, a topic that we have emphasized in our research group since reporting the work of Zalusky et al. using poly(lactide)-containing block copolymers in 2001.⁷ In section 4, new techniques for preparing nanoporous materials using block copolymer templates are introduced and summarized. As this field has developed, there have been new and innovative methods for removing components from self-assembled block copolymers. We also cover nanoporous materials made using exogenous porogens, such as supercritical carbon dioxide, and an appropriately designed block copolymer. In the penultimate section 5, we cover nanoporous membranes from block copolymer precursors, an emerging and technologically relevant area of research. Section 6 gives a brief summary and outlook.

2. Nanolithography

Block copolymer lithography employing nanoporous templates has received significant attention in the past decade as a means to enable the development of future technologies.⁸ For the microelectronics industry, the shrinking size of electronic devices requires the use of ever-smaller templates.⁹ Evidence of this is the fact that IBM recently announced the use of PS-PMMA^a derived nanolithography templates for the fabrication of air gaps as a solution to low dielectric constant systems in every microprocessor system they produce, starting in 2009.¹⁰

^aAbbreviations: AFM, atomic force microscopy; APTES, 3-aminopropyltriethoxysilane; ATRP, atom-transfer radical polymerization; BET, Brunauer–Emmett–Teller; BJH, Barrett–Joyner–Halenda; CMOS, complementary metal oxide semiconductor; DETA, diethylenetriamine; DHN, 1,5-dihydroxynaphthalene; DNA, deoxyribonucleic acid; FESEM, field-emission scanning electron microscopy; SEM, scanning electron microscopy; FFT, fast Fourier transform; HDMS, hexamethyldisilazane; HFPD, 2,2,3,3,4,4-hexafluoro-1,5-pentanediol; MCPBA, *m*-chloroperoxybenzoic acid; Mn, number-average molecular weight; MUA, 11-mercaptopentadecanoic acid; NMR, nuclear magnetic resonance; P2VP, poly(2-vinylpyridine); P4VP, poly(4-vinylpyrrolidone); PAA, poly(acrylic acid); PAN, poly(acrylonitrile); PB, poly(1,2-butadiene); PBCB, polyvinylbenzylcyclobutene; PCL, poly(ϵ -caprolactone); PDI, polydispersity index; PDMA, poly(*N,N*-dimethylacrylamide); PDMS, poly(dimethylsiloxane); PE, polyethylene; PEO, poly(ethylene oxide); PFES, polyferrocenylsilane; PFMA, poly(perfluorooctylethyl methacrylate); PFS, poly(4-fluorostyrene); PI, polyisoprene; PLA, poly(D,L-lactide); PLLA, poly(L-lactide); PMMA, poly(methyl methacrylate); PPFS, poly(pentafluorostyrene); PPG, poly(propylene glycol); PS, polystyrene; RAFT, reversible addition-fragmentation chain transfer; RIE, reactive ion etch; *R*-MMA, (*R*-(+)-3-methyladipic acid; SAXS, small-angle X-ray scattering; scCO₂, supercritical carbon dioxide; SEC, size-exclusion chromatography; SEM, scanning electron microscopy; SFM, scanning force microscopy; TC, trithiocarbonate; TEM, transmission electron microscopy; T_d, depressurization temperature; T_g, glass-transition temperature; TGA, thermal gravimetric analysis; THF, tetrahydrofuran; TOES, tetraethoxysilane; TOF-SIMS, time-of-flight secondary-ion mass spectrometry; UV, ultraviolet; VUV, vacuum ultraviolet; XPS, X-ray photoelectric spectroscopy.

The nanoscale domain spacing and ability to control structure and periodicity make block copolymer derived nanolithographic templates ideal for such applications.

(a) Development and Applications of Block Copolymer Templates. The workhorse of block copolymer templates in nanolithographic applications have been poly(styrene)-*b*-poly(methylmethacrylate) (PS-PMMA) block copolymers. These materials have been widely studied, developed, and advanced by Russell and co-workers since the turn of the century.¹¹ As such, the first half of this subsection will focus on the development and application of these PS-PMMA based templates. Along with the development of traditional PS-PMMA template materials, new templating copolymer systems are under development. The second half of this subsection will discuss the development of these “nontraditional” templating systems.

Melde et al. utilized PS-PMMA diblock copolymer thin film templates to prepare silicon oxide nanostructures.¹² Two alternative strategies to fabricate silicon oxide nanostructures using a selective mineralization sol–gel approach were also disclosed, but will not be discussed here. Silicon oxide is useful as a coating or substrate because of its hardness, transparency in the visible spectrum, and low dielectric constant. The PS-PMMA diblock material used had a total number-average molecular weight of 50 kg mol⁻¹ and PS volume fraction of 0.70. Silicon oxide was grown in a nanoporous PS thin film. The porous thin film was prepared by (1) spin coating the diblock materials onto a silicon substrate and (2) selectively etching the PMMA using UV light followed by an acetic acid rinse (a standard protocol for PS-PMMA block copolymers). The material was then exposed to tetraethoxysilane (TOES) and 5 M HCl vapors at 75 °C for 3.5 h. This vapor exposure was followed by calcination at 500 °C for 5 h under air. Nanostructures that were uniform in height and diameter were observed, although the pores were not completely filled. Longer vapor exposure times of 4 h were investigated, but this led to overfilling of the pores, which formed “mushroom” structures after calcination. Immersion of the porous PS template in a TEOS sol was also investigated. After being submerged for a total of 42 h, the pores were partially filled and uniform nanopost arrays were evident. The utility of these nanostructured silicon oxide surfaces as precursors to ultrahydrophobic surfaces was investigated. Nanopost arrays were functionalized by a vapor phase reaction with trimethylchlorosilane or (tridecafluoro-1,1,2,2-tetrahydrooctyl)dimethylchlorosilane. The native oxide surfaces of silicon wafers were also modified with these organosilanes for comparison purposes. Dynamic contact angle measurements showed a notable hysteresis in the nanostructured surface contact angles, which was not evident in the flat native oxide functionalized surfaces. The authors suggest that this hysteresis indicates a “pinning” of the water droplets, caused either by surface roughness or chemical heterogeneities over the nanostructured surfaces. This methodology represents an important proof of principle that could be applied to other block copolymers, such as polystyrene-*b*-poly(ethylene oxide) (PS-PEO), for the preparation of a variety of other important metal oxide nanoarrays.

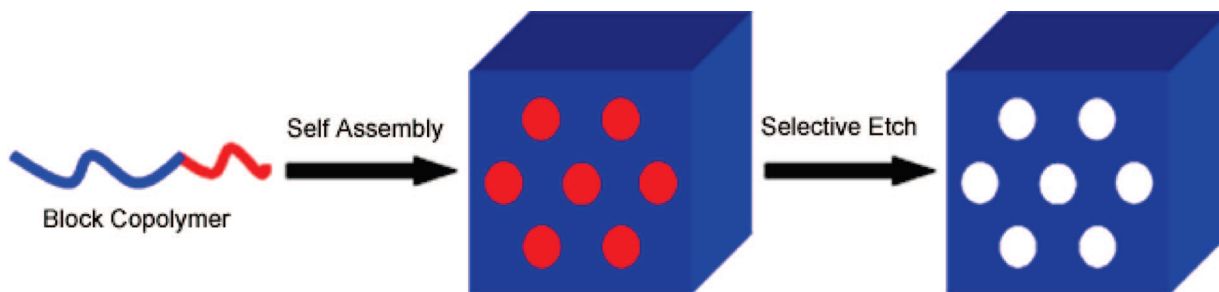


Figure 1. Schematic representation of the formation of nanoporous polymeric materials from ordered block copolymers.

In 2006, Zschech et al. demonstrated the use of PS-PMMA block copolymers as lithographic masks for the preparation of highly ordered arrays of gold nanoparticles.¹³ Nanoporous silicon nitride-coated silicon wafers were prepared by first coating a silicon wafer with a 35 or 60 nm thick layer of silicon nitride. A hydroxyl terminated PS-PMMA random copolymer was then grafted to the nitride surface. After grafting, a PS-PMMA diblock material with a total number-average molecular weight of 67 kg mol⁻¹ and PS volume fraction of 0.70 was spin-coated onto the random copolymer surface from toluene. The films were annealed at 165 °C for 2 days, and the oriented PMMA cylinders were selectively etched using UV irradiation followed by acetic acid rinsing. The nanoporous PS template was then stained with ruthenium tetroxide to increase its etch contrast. Dry plasma etching was then used to transfer the template pattern into the underlying silicon nitride layer. A 20 nm thick layer of gold was deposited onto the patterned substrate by thermal vacuum evaporation. Finally, the nanoporous PS template was manually removed using a sharp blade. The resulting immobilized gold nanoparticle arrays were examined by scanning electron microscopy (SEM). Direct examination of the images showed that the nanoparticles had a diameter of 15 nm, whereas Fourier transform analysis was used to determine a nearest neighbor distance of 41 nm. The lateral density of the particles was 6.87×10^{10} nanoparticles cm⁻² and the arrays remained stable up to 600 °C. Conceivably, this methodology could be applied to nanoparticles of other metals, such as silver, platinum, and palladium, or any other metal precursor that could be reduced inside the nanopores.

More recently, Zschech et al. described a similar method, compatible with complimentary metal oxide semiconductor (CMOS) technology, to prepare ordered arrays of silicon nanorods with the <100> direction perpendicular to the surface of a (100) silicon wafer.¹⁴ The techniques used to prepare the polymer template were identical to those used in the authors' 2006 publication, with the major exception being that the polymer template was prepared from a PMMA majority PS-PMMA material. The PS-PMMA material had a total number-average molecular weight of 70.7 kg mol⁻¹ with a PS volume fraction of 0.30. Silicon nitride was coated onto a silicon wafer and a PS-PMMA random copolymer was grafted onto the silicon nitride surface, as done previously. The diblock copolymer was spin-coated onto the grafted surface, annealed, and the PMMA was selectively etched using the standard UV/acetic acid procedure. Once the template was formed, the pattern was transferred into the underlying silicon nitride layer using reactive ion etching

(RIE). Silicon nitride dots formed at the position of the PS dots, exposing the underlying silicon between the dots. The exposed silicon was finally etched with HBr for 60 s and silicon nanorods formed at the position of the silicon nitride dots. By combining the advantages of block copolymer lithography with a CMOS technology compatible method, this procedure offers an avenue for the technical exploitation of silicon nanowires.

One challenge with conventional templated selective etching techniques for the formation of nanoporous materials has been the tedious additional physical or chemical treatments required to completely remove the residual material following its use as a template. Hozumi et al. described the use of vacuum ultraviolet (VUV) light for selective etching to both prepare well-defined nanoporous arrays from PS-PMMA diblock copolymers and subsequently eliminate the remaining nanoporous PS template.¹⁵ A PS-PMMA diblock material with a total number-average molecular weight of 60.8 kg mol⁻¹ and PMMA volume fraction of 0.30 was cast from a 3 wt % toluene solution onto a silicon substrate. Following annealing at 170 °C for 24 h, the films were exposed to 172 nm VUV light for 5–70 min at a reduced pressure of either 10 or 1×10^3 Pa. The two reduced pressures produced atmospheres with varying amounts of residual air. Nanopore formation and decomposition of the remaining nanoporous film was investigated by atomic force microscopy (AFM), X-ray photoelectric spectroscopy (XPS), and field-emission scanning electron microscopy (FESEM). Etching for 20 min at a residual pressure of 10 Pa produced well-defined 15 nm diameter hexagonal nanopore arrays in a PS matrix shown in Figure 2. Etching the same nanoporous film for an additional 40 min produced a surface with carbon, oxygen, and silicon concentrations (determined by XPS) similar to the silicon substrate, indicating complete removal of the nanoporous PS film. This strategy demonstrated controlled nanoarray formation and subsequent template elimination, without tedious physical or chemical treatment.

Asakura et al. followed up this initial publication with a report which used these techniques to fabricate copper nanodot arrays.¹⁶ A nanoporous PS template was fabricated using the same PS-PMMA material and techniques described above. A VUV light irradiation time of 30 min was used to selectively degrade PMMA leaving a porous PS template with pores approximately 20 nm in diameter and 6 nm deep. The nanoporous film was then modified with an amino-terminated organosilane by chemical vapor deposition. XPS indicated that VUV treatment caused the formation of hydroxyl groups on the surface of the PS matrix and the

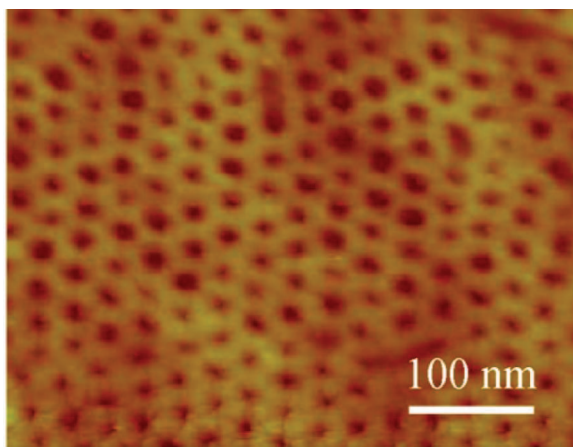


Figure 2. AFM image of nanoporous PS film prepared from VUV light etching of PS-PMMA. Reprinted with permission from ref 15. Copyright 2005 Elsevier.

organosilane consequently adsorbed to the top of the PS template as well as the desired exposed silicon substrate. However, the organosilane-PS surface on the top of the template was successfully removed by sonicating the film in toluene for 10 min (this treatment could presumably have an effect on the template pore diameter, but this point was not discussed by the authors). The organosilane modified template was then immersed in a 1.4 mM chloride-rich Pd(II) solution for 20 min. The sample was rinsed and immediately immersed in a copper electrolysis plating solution. Finally, the template was exposed to 30 min of additional VUV light at 1×10^3 Pa to remove the remaining PS template. AFM demonstrated the formation of copper nanodots 10–25 nm in diameter and 3.0–4.2 nm high. These structures could be useful for the development of new nanodot-based devices, such as magnetic recording media. However, it should be noted that these techniques do require etching under a vacuum, which may limit the practical applicability to some extent.

Expanding on the techniques of traditional nanolithography, there have been several recent examples of using diblock copolymer derived nanoporous templates for the patterned deposition of a variety of nanoparticles. In 2005, Zhang et al. reported an electrophoretic process for the deposition of CdSe nanoparticles into PS-PMMA derived nanopore and nanotrench templates.¹⁷ Two PS-PMMA diblock materials were used. The first material exhibited a cylindrical morphology with a total number-average molecular weight of 66.0 kg mol⁻¹ and a PMMA volume fraction of 0.25. The second material exhibited a lamellar morphology with a total number-average molecular weight of 93.0 kg mol⁻¹ and a PMMA volume fraction of 0.50. Templates were formed by spin-coating these copolymers from toluene solutions onto a silicon substrate modified with a PS-PMMA random copolymer (58 mol% PS). Templates were typically 30–40 nm in thickness with feature sizes on the order of 15 nm. Following spin-coating, the films were annealed at 170 °C and the PMMA was selectively degraded under deep ultraviolet (UV) irradiation ($\lambda = 254$ nm) for 30 min. The templates were then floated onto carbon-coated copper grids, which served as the anode for electrophoretic deposition. The

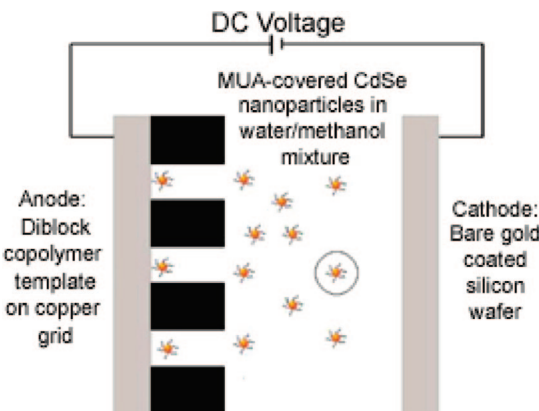


Figure 3. Apparatus used to deposit CdSe nanoparticles into diblock copolymer templates. Reprinted with permission from ref 17. Copyright 2005 American Chemical Society.

cathode consisted of bare gold-coated silicon wafers. This apparatus was then placed in a deposition bath filled with a solution of 11-mercaptopoundecanoic acid (MUA)-covered CdSe nanoparticles in water and methanol. A dc voltage was applied between the two electrodes to drive the negatively charged CdSe nanoparticles into the diblock copolymer templates. The optimal field strength was 0.4–0.8 V cm⁻¹, with a typical nanoparticle concentration of approximately 1×10^{13} particles mL⁻¹ and deposition time from 1 to 10 min. These conditions were used to selectively deposit CdSe nanoparticles into both nanoporous and nanotrench templates (Figure 3). The authors demonstrated that the photoluminescence of the nanoparticles was maintained following the electrophoretic deposition.

Zhang et al. followed up this work by publishing a related paper on templating PEO-functionalized CdSe nanoparticles.¹⁸ Once again, PS-PMMA derived thin film templates were used. The PS-PMMA materials had total number-average molecular weights of 140 and 260 kg mol⁻¹ and contained 68 and 50 wt% PS, respectively. The PEO-covered CdSe nanorods, 20–60 nm in length and 7–8 nm in diameter, were prepared by refluxing alkane covered rods in pyridine followed by refluxing in methanol with thiol-terminated PEO. Nanopore and nanotrench templates were fabricated from the two diblock samples using methods analogous to those described in the authors' previous publication.¹⁷ The templates were floated onto copper transmission electron microscopy (TEM) grids, which were then placed into an aqueous solution of the PEO-covered nanorods. TEM was used to examine the resulting deposition of the nanorods into the templates (Figure 4). The PEO-covered nanorods accumulated both on the PS template surface as well as within the template. For the case of the nanotrench templates, the nanorods aligned themselves with the channel walls. The deposition into the nanopore templates was quite efficient when the length of the rod was less than the pore diameter, but was reduced when the rod length exceeded the pore diameter. Finally, the authors investigated the surface affinity of the PEO-CdSe nanorods by investigating the deposition of MUA-functionalized CdSe nanorods. Although both materials are water soluble, the MUA materials could not be deposited into the copolymer templates. The authors used

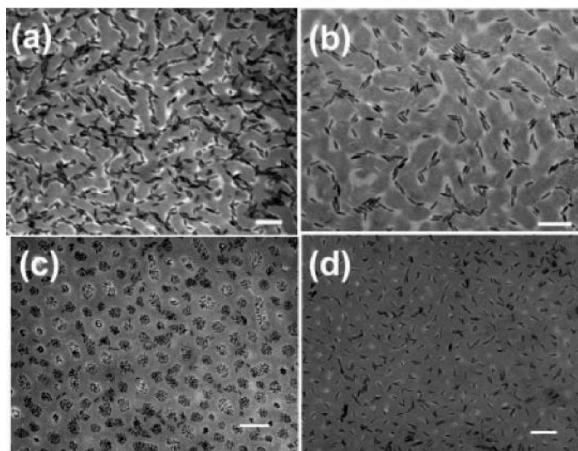


Figure 4. TEM images of (a) 25 and (b) 35 nm long PEO-covered CdSe nanorods on a nanoporous lamellar template; (c) 20 and (d) 40 nm long PEO-covered CdSe nanorods on a nanoporous cylindrical template (the scale bars represent 100 nm.) Reprinted with permission from ref 18. Copyright 2006 American Chemical Society.

this result to suggest that the surface activity of PEO was required “to aid the segregation of the nanorods to the water–air interface, where they are absorbed by the templates.” Together, these two examples describe an impressive methodology that is somewhat universal with regard to template and nanoparticle structure. We agree with the authors forecast that it could be potentially useful for important electronic and photoactive applications.

Patterning magnetic materials using nanoporous block copolymer templates has also been investigated. For example, in 2005 Darling et al. used a cylindrical forming PS-PMMA diblock material as a template to prepare organized assemblies of magnetic FePt nanoparticles.¹⁹ FePt particles were of particular interest because their chemical and magnetic stability make them likely candidates for the preparation of ultrahigh-density recording media. The PS-PMMA diblock material used had a total number-average molecular weight of 77 kg mol⁻¹ with a PMMA weight fraction of 0.29. The diblock material was spin-coated from toluene onto a fresh silicon nitride substrate and annealed at 24 °C for 6 h to allow the formation of PMMA cylinders parallel to the substrate surface. The PMMA was then selectively etched using VUV radiation. FePt nanoparticles (oleic-acid-capped) were then spin-coated from octane onto the nanoporous template. AFM analysis demonstrated that 99% of the nanoparticles adhere to the nanochannel surface, as shown in Figure 5. Because these methods do not rely on the magnetic character of the FePt core, they could also be used for templating applications in electronic, photonic, and catalytic fields.

In 2006, Bandyopadhyay et al. were the first to demonstrate the spontaneous deposition of DNA-functionalized gold nanoparticles onto functionalized nanoporous templates from block copolymers.²⁰ The nanoporous templates were prepared from two PS-PMMA diblock materials having total number-average molecular weights of 77 and 147 kg mol⁻¹ and PS volume fractions of 0.72 and 0.77, respectively. The templates were prepared in the usual manner, by spin-coating a polymer solution onto a PS-PMMA random copolymer-coated silicon substrate, annealing the substrate at 165 °C

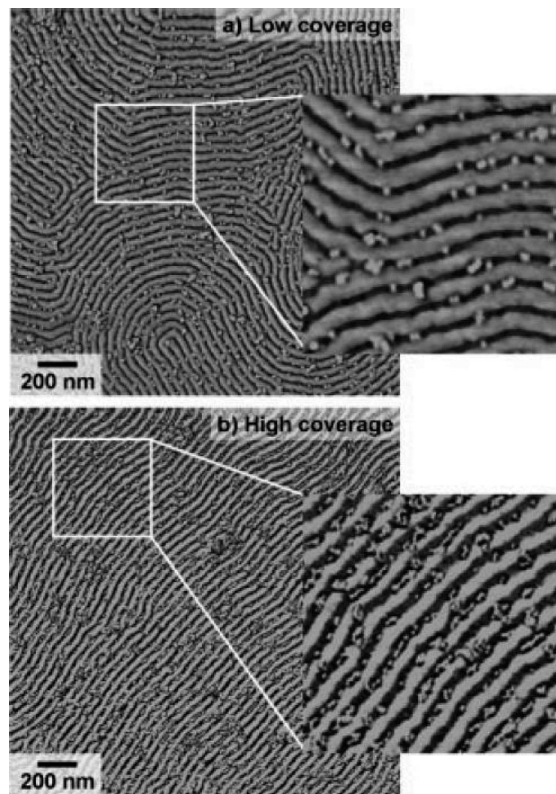


Figure 5. AFM images showing selective adsorption of single FePt nanoparticles onto VUV light etched templates with a) low coverage and b) high coverage. Reprinted with permission from ref 19. Copyright 2005 Wiley-VCH Verlag & Co. KGaA.

for 2 days, and then selectively etching the PMMA with the traditional UV/acetic acid treatment. This procedure yielded a nanoporous PS template deposited on top of a silicon substrate, with the pores completely extending to the SiO_x surface, as supported by AFM. Both native and neutralized silicon substrates were investigated. Three forms of surface neutralization approaches were investigated: PS-PMMA random copolymer neutral brushes, alkylchlorosilanes, and hydrogen passivation. By using 77 or 147 kg mol⁻¹ PS-PMMA material, nanoporous films with average center-to-center pore spacings of 51 and 66 nm and pore diameters of 23 and 33 nm were obtained.

The authors’ approach for deposition was based on introducing intrinsic attractive parameters through chemical modification of the SiO_x surface at the bottom of each nanopore (Figure 6). Thus, the SiO_x surface was either simply functionalized with a positively charged aminosilane, such as diethylenetriamine (DETA) or 3-aminopropyltriethoxysilane (APTES), or further functionalized with probe oligonucleotides. DNA-Au nanoparticles were prepared by reducing HAuCl₄ with sodium citrate followed by reaction with thiol-terminated oligonucleotides. Diameters of the hydrated and dehydrated Au nanoparticles were approximately 30 and 18 nm, respectively. For aminosilane-functionalized substrates, optimal deposition was obtained using a template that was prepared from the lower-molecular-weight PS-PMMA material that was spin-coated onto a hydrogen-passivated silicon substrate and briefly rinsed with 5% HF. AFM analysis showed that no more than a single nanoparticle was immobilized per nanopore. For oligonucleotide-functional-

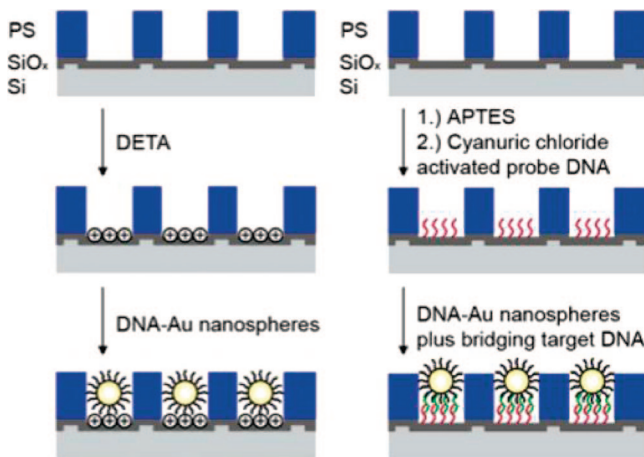


Figure 6. Schematic representations of two functionalization approaches used for the deposition of DNA in diblock copolymer derived templates. Reprinted with permission from ref 20. Copyright 2006 American Chemical Society.

ized substrates, a complimentary bridging target DNA was added to the deposition media to facilitate targeted deposition. Although deposition using this probe oligonucleotide process was much more selective for the nanopore, the percentage of the total number of nanopores filled was considerably less than the percentage obtained on the aminosilane functionalized substrates. Nevertheless, the feasibility of a rapid (1–2 h) deposition process that uses small volumes of DNA-Au nanoparticles (compared to dip or spin-coating processes) was demonstrated. We are optimistic about the potential impact this methodology could have on numerous biological applications and see it as an important proof of principle.

Although PS-PMMA diblock copolymers are the materials most widely used to fabricate nanoporous polymeric templates or for nanopattern transfer, other block copolymers have been investigated for the same purposes. These newer materials often bring distinct features that can be useful for these applications. For example, Fu et al. synthesized poly(pentafluorostyrene)-*b*-PMMA (PPFS-PMMA) diblock copolymers using atom-transfer radical polymerization (ATRP) for the purpose of fabricating nanoporous ultralow-dielectric constant materials for the development of next-generation high-density circuits.²¹ First, the pentafluorostyrene was polymerized in bulk (using ethyl bromoisobutyrate as the initiator with copper(I) bromide catalyst and 2,2'-bipyridine as the ligand at 110 °C), the polymer was then purified to remove traces of copper, and finally precipitated into methanol. The bromo-terminated PPFS macroinitiator was then dissolved in xylenes and ATRP of MMA was initiated at 90 °C with the same catalyst and ligand conditions. Three PPFS-PMMA diblock materials were prepared using this procedure. Total number-average molecular weights ranged from 62 to 83 kg mol⁻¹ with polydispersity index (PDI) below 1.3 for all three samples. The amount of PMMA ranged from 16 to 37 wt %. The block composition of the copolymers was confirmed by NMR spectroscopy as well as time-of-flight secondary-ion mass spectrometry (TOF-SIMS). TOF-SIMS clearly showed units composed of PFS bonded to MMA. Following preparation of the PPFS-PMMA materials, they were spin-coated from *N*-methyl-2-pyrroli-

done onto a silicon substrate and annealed at 170 °C for 12 h (the morphology of these materials was not reported). The film was subsequently exposed to UV radiation to selectively degrade the PMMA, leaving a porous film with pore diameters of 30–50 nm. The porosity of the nanoporous films was determined by Brunauer–Emmett–Teller (BET) analysis, and the dielectric constants were measured. A nanoporous film prepared from a diblock with 29 wt % PMMA demonstrated a pore volume of 0.29 mL g⁻¹ and a dielectric constant of 1.8. For comparison, the dielectric constant of a pristine PPFS film was 2.2. Thus, the utility of block copolymers for the fabrication of ultralow dielectric constant materials, which are of great interest to the microelectronics industry, was demonstrated.

Continuing on the theme of low-dielectric-constant materials and building off of the research of Hedrick and co-workers,²² Chung et al. described the synthesis of low dielectric nanoporous materials from triblock copolymers consisting of a thermally stable polyimide block and two thermally labile poly(propylene glycol) (PPG) blocks.²³ Triblock materials were prepared by reacting a PPG material possessing a single aryl amine endgroup with *p*-phenylene diamine and a spiro dianhydride. The resulting triblock consisted of a polyimide middle block with PPG blocks on either side. Three triblock copolymers were prepared with PPG incorporation of 8–20 wt%, determined by both NMR spectroscopy and thermal gravimetric analysis (TGA), with overall number-average molecular weights ranging from 44.7 to 68.4 kg mol⁻¹. TGA analysis demonstrated that thermal decomposition of PPG began at 210 °C and the polyimide thermally decomposed at 410 °C. Therefore, thermolysis of the PPG was performed by heating the samples at 240 °C under reduced pressure. The absolute pressure was critical for the formation of a nanoporous polyimide material. When the pressure was not reduced, significant pore collapse was noted. The authors suggested that the pore collapse was being caused by plasticization of the polyimide by the PPG degradation products, and the reduced pressure assisted in the diffusion of the degradation products out of the polyimide matrix. Using a reduced pressure of 95 kPa, researchers produced porous materials with pore diameters between 100 nm and 1 μm, depending on the triblock materials that was used. Dielectric constants of these materials were 2.42–2.60, compared to 2.73 for a nonporous polyimide film. Both of the two previous methodologies could be used as more general methods for the preparation of low-dielectric-constant materials for the microelectronics industry.

Diblock copolymer templates have also been used to prepare various nanoporous inorganic materials. These nanoporous inorganic networks are potentially very useful because they combine the high surface area of a nanoporous material with the potentially catalytic and conductive properties of an inorganic material. Lu et al. prepared a nanoporous titania film using a template formed from blending a polystyrene-*b*-polyisoprene (PS-PI) diblock copolymer with a PS homopolymer.²⁴ The PS-PI diblock material and PS homopolymer had total number-average molecular weights of 266 and 10 kg mol⁻¹, respectively. The blend was prepared in solution using toluene, with the total volume

fraction of PI being 0.34. The PI was selectively etched in an ozone atmosphere for 36 h, followed by a 12 h rinse in ethanol. The resulting template possessed a disordered bicontinuous structure with the void phase 50 nm wide and the PS network 100 nm wide. Upon formation of the nanoporous network, it was immersed in a titania precursor solution (a mixture of titanium tetraisopropylate and acetylacetone) and subjected to constant 200 rpm rotation for 3 weeks. After the 3 week immersion time, complete infiltration was observed by SEM. The remaining PS template was removed by calcination at 500 °C for 3 h. SEM analysis of the titania network showed that it was 20–30 nm in diameter, slightly smaller than the original 50 nm voids in the nanoporous templates. The surface area of the network, as measured by BET analysis, was 53 m² g⁻¹. This value is nearly identical to the network surface area of Degussa P25, a widely used commercial titania photocatalyst. The photocatalytic performance of the titania network relative to Degussa P25 was evaluated by investigating two model photocatalytic reactions: the gas-phase oxidation of NO and the liquid-phase degradation of methylene blue. Titania network demonstrated a catalytic performance similar to that of Degussa P25 in both reactions, with the titania network offering advantages of ease of material handling and recycling efficiency (although the 3 week immersion time will need to be addressed to make the material commercially attractive).

The majority of the examples described thus far have relied on either relatively harsh etching conditions (strong acids or calcination) or UV irradiation that lead to a cross-linked matrix. More chemically benign methods for etching the sacrificial block, such as ester hydrolysis, have also been investigated. Olayo-Valles et al. systematically investigated the use of polystyrene-*b*-poly(D,L-lactide) (PS-PLA) diblock copolymers to achieve perpendicular cylindrical domain orientation in thin film templates.²⁵ Several variables, including molecular weight, film thickness, annealing temperature, and substrate, were investigated. PS-PLA samples with total number-average molecular weights of 60.5 and 96.0 kg mol⁻¹ and PLA volume fractions of 0.29 and 0.36, respectively, were primarily investigated. Films were prepared by spin-coating from chlorobenzene onto a silicon substrate with native oxide layer. Film thickness varied from 24 to 324 nm for the higher-molecular-weight sample, and from 14 to 257 nm for the lower molecular weight sample. Annealing temperatures ranged from 110 to 240 °C for 12 h. Regardless of molecular weight or annealing temperature, a perpendicular orientation was achieved when the film thickness was greater than the repeat spacing of the bulk morphology. The authors explained that this is due to the similar surface energies of PS and PLA. In fact, when a lamellar sample was subjected to similar conditions, it too displayed a perpendicular orientation, which has been shown to occur only when the surface energies of the two components are similar.²⁶ Finally, the effect of the substrate surface was investigated. Films were prepared in an identical manner using Al₂O₃, GaAs, and MgO single-crystal substrates, polycrystalline Al, Au, Cu, Ni₅₀Mn₅₀, and SiO₂ seed layers, and hydrogen peroxide or hexamethyldisilazane (HDMS)-

modified silicon surfaces as substrates. All substrate surfaces demonstrated the same perpendicular orientation behavior.

Selective chemical etching of the PLA blocks described above using a 0.5 M NaOH solution in a mixture of water and methanol was investigated. Films cast onto silicon substrates with their native oxide layer were readily etched; however, the film delaminated from the substrate. When the hydrophobic HDMS treated substrate was used, no delaminating problems were encountered. Given the hydrophobic nature of the surface, PS is expected to be at the film–substrate interface, allowing for better adhesion. A two-step process for preparing nanolithography templates was subsequently developed. First, the PLA was partially degraded to obtain nanopitted films. Second, O₂ RIE was used to complete the path of the pores through the substrate. Given that the PS was not cross-linked, the remaining PS template could be removed by simple dissolution. This method was subsequently used to prepare a substrate with nanopits. Fabrication of structures with higher aspect ratios may be possible by using thicker films.

Lo et al. described the use of techniques similar to those used by Olayo-Valles et al.²⁵ and nearly identical to those reported by Johnson et al.²⁷ to prepare CdS nanoarrays using nanoporous templates derived from polystyrene-*b*-poly(L-lactide) (PS-PLLA) diblock copolymers.²⁸ The PS-PLLA material had a total number-average molecular weight of 53.9 kg mol⁻¹ with a PLLA volume fraction of 0.25. Hydroxyl terminated PS was prepared using controlled radical techniques followed by ring-opening polymerization to form the PLLA block. The polymer was spin-coated onto glass from toluene and the resulting film was exposed to UV radiation for 10 min to cross-link the PS and increase adhesion to the glass substrate. PLLA was subsequently etched using the same 0.5 M NaOH procedure described above. The CdS nanocrystals were generated *in situ* by exposing the template incorporated with cadmium sulfate to H₂S vapor. Three different pore-filling techniques were described. First, the template was placed under a vacuum to remove air in the pores, followed by the addition of a 0.48 M cadmium sulfate water/methanol solution. The second method involved the removal of the glass substrate using a 1% HF solution, collecting the film on a copper grid and then immersing the grid supported film into the same cadmium sulfate solution. In the final method investigated, the template was directly floated onto the cadmium sulfate solution. The templates were rinsed with water, dried, and then exposed to H₂S vapor to reduce the cadmium sulfate to the desired CdS nanostructures. UV and photoluminescence experiments indicated that the third pore-filling method produced arrays that showed the highest amount of optical activity. The *in situ* CdS nanocrystal formation coupled with soft etching methods make this a potentially useful route to quantum dot nanoarrays.

In a related work, Crossland et al. described the synthesis of freestanding nanowire arrays from poly(4-fluorostyrene)-*b*-poly(D,L-lactide) (PFS-PLA) diblock copolymer derived templates.²⁹ The PFS-PLA sample used was again prepared using a combination of controlled ring opening and reversible addition–fragmentation chain transfer (RAFT) polymeriza-

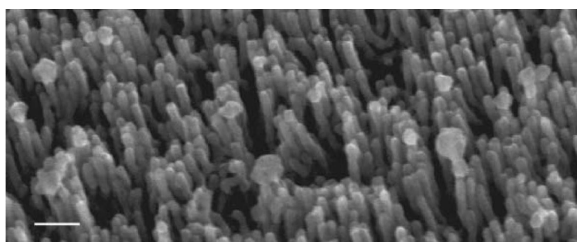


Figure 7. SEM image of freestanding copper nanowires following degradation of the PFS matrix (the scale bar represents 100 nm). Reprinted with permission from ref 29. Copyright 2007 The Royal Society of Chemistry.

tion techniques. The material had a total number-average molecular weight of 30.0 kg mol^{-1} and contained 30 wt % PLA. Differential scanning calorimetry (DSC) analysis of the diblock material showed two distinct glass-transition temperatures at 57 (PLA) and 103 °C (PFS). Small-angle X-ray scattering (SAXS) analysis gave a principal domain spacing of 26 nm. PFS-PLA films, approximately 300 nm thick, were prepared by spin-coating the polymer onto gold-coated silicon substrates. The PLA microdomains were subsequently aligned normal to the substrate using an electric field (the free energy of the system is reduced when material interfaces with differing dielectric constants align parallel to the electric field vector). Electric fields were applied while the sample was annealed at 140 °C for 35 h. The strength and duration of the electric field were shown to play important roles in alignment. Fields that were either too weak or too short resulted in PLA domains that either did not span the entire film thickness or formed disorganized structures. PLA was subsequently etched from aligned films using the previously described NaOH conditions, and the remaining nanoporous PFS film did not delaminate from the gold surface. AFM analysis of the template showed a highly ordered structure with an average cylinder diameter of 15 nm and an average center-to-center distance of 32 nm. Using electrochemical deposition methods, Cu_2O was deposited into the cylindrical pits of the template, forming freestanding nanowire structures shown in Figure 7. Two methods of removing the remaining PS template were investigated: dissolution in toluene or UV degradation. Solvent dissolution resulted in bunching of the nanowires, whereas UV degradation minimized this effect. Further development of these soft etch methodologies will open the door to nanoscale templating of functional polymer systems, such as conjugated polymers for photovoltaic applications.

Although the demonstrated and potential utility of AB diblock copolymers in nanolithography is remarkable, there are only a limited number of structures adopted by diblock copolymer thin films. Therefore, the use of triblock terpolymer materials has been investigated. Guo et al. expanded on the work of Olayo-Valles et al. by preparing PS-PI-PLA and PI-PS-PLA triblock terpolymers and exploring their thin film behavior and applicability as nanoporous templates.³⁰ The authors envisioned a core–shell morphology in a thin film, with the cylinders oriented perpendicular to the substrate, which could be used as a nanoring template. First, a PS-PI-PLA material with total number-average molecular weight of 65.0 kg mol^{-1} and PI and PLA weight fractions

of 0.11 and 0.29 was investigated. As previously described, films were spin-coated onto a HDMS modified silicon surface, annealed at 150 °C for 15 h, and analyzed by AFM.²⁵ Hexagonally packed regions of a core–shell cylindrical morphology, with PLA in the core and PI in the shell, were readily apparent. The mean center-to-center distance was 65 nm. Attempts to selectively remove the PI shell by ozonolysis and generate the desired nanoring template led to concomitant partial removal of the PLA component. The partial success of these efforts suggested that the related PI-PS-PLA material could lead to the desired core–shell morphology. The triblock material had a total number-average molecular weight of 18.0 kg mol^{-1} with PI and PLA weight fractions of 0.32 and 0.30. Thin films of this material were prepared in a manner similar to that described for the PS-PI-PLA materials above. Although SAXS analysis of the material suggested a hexagonal morphology, AFM did not show the clear core–shell morphology. SEM analysis of the material, stained with OsO₄, was consistent with a core–shell morphology, with PI forming the core and PS forming the shell in a matrix of PLA. This time, ozonolysis treatment selectively degraded the PI, leaving the PLA untouched. Further degradation in 0.05 M water/methanol NaOH solution left the desired nanoscopic, hollow, cylindrical PS “nanobushing.” This work demonstrated that the use of triblock terpolymers could significantly expand the utility of block-copolymer-based templating and pattern-transfer methods, leading to the fabrication of more complicated structures.

Bang et al. provided another example of a triblock terpolymer approach to the preparation of nanoporous thin films, using PEO-PMMA-PS triblock materials.³¹ Rather than investigate more complicated morphologies, the authors’ approach sought to “combine the facile degradation of PS-PMMA with the long-range lateral order of PS-PEO-based systems.” The triblock materials investigated were synthesized by RAFT polymerization. A PEO-RAFT macroinitiator was prepared by reacting monomethoxy PEO (5.0 kg mol^{-1}) with α -bromophenylacetic acid followed by reaction with phenylmagnesium bromide and carbon disulfide to yield the dithioester macroinitiator. Addition was confirmed by NMR spectroscopy and size-exclusion chromatography (SEC). Reaction of the PEO macroinitiator with azobisisobutyronitrile and MMA, followed by reaction with styrene yielded the desired PEO-PMMA-PS triblock materials. A library of materials was prepared with overall number-average molecular weights of $20.0\text{--}121.0 \text{ kg mol}^{-1}$, with styrene as the majority block, and PMMA volume fractions of 0.07–0.16. The morphologies of three selected triblock materials, with PMMA volume fractions between 0.07 and 0.13, were investigated. The materials were spin-coated onto silicon substrates and annealed in benzene vapor, yielding well-defined arrays of cylindrical microdomains of the minor components oriented perpendicular to the surface (Figure 8). The wafer–polymer interface was also investigated and the same morphology was observed. The domain spacing calculated by SFM and SAXS are in general agreement in all cases.

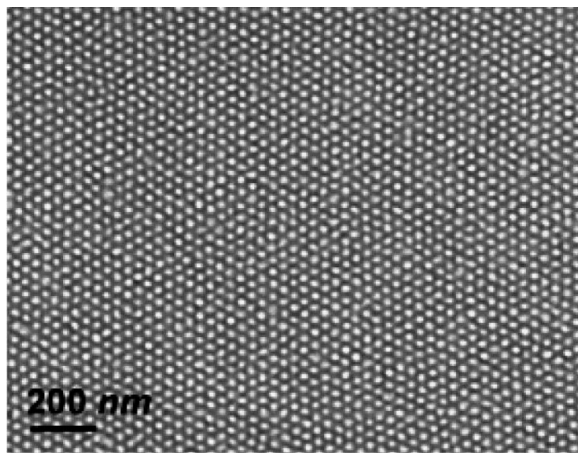


Figure 8. TEM image of nanoporous thin film derived from a PEO-PMMA-PS triblock terpolymer. Reprinted with permission from ref 31. Copyright 2006 American Chemical Society.

The selective etching of the PMMA block was investigated next. Samples were exposed to deep UV irradiation followed by acetic acid rinsing. Interestingly, the authors noted a window of optimal PMMA molecular weight. When the PMMA molecular weight became too small, it became miscible with PEO and a single cylindrical domain was formed. Previous work has shown that the presence of ether-containing solvents retards the UV degradation of PMMA, so limited PMMA degradation was expected for these mixed PEO-PMMA samples. On the opposite side of the molecular weight spectrum, when the PMMA molecular weight became too large, long-range ordering was not obtained. Using the optimal PMMA molecular weight range, the researchers prepared hexagonal array templates with 10–15 nm diameter cylinders. The ability to tune the complex phase morphologies of triblock terpolymer systems, by varying block length and composition, makes them a powerful tool for nanolithography. More generally, this example demonstrates the benefit of triblock materials to “combine” attributes of multiple diblock systems into a single system. This combination could ultimately lead to improved material performance and morphological control.

(b) Directed Assembly. The preceding discussion focused on the use of block copolymer self-assembly to form nanostructures that hold significant potential for use as templates or scaffolds for the fabrication of large area arrays of inorganic nanostructures that have relevance in the microelectronics industry. A central requirement for use in these applications is the ability to achieve long-range order and precisely control the placement of the nanoscale domains. Multiple methods have been investigated to achieve such control. To date, three general strategies have been investigated: chemical modification of the substrate, physical patterning of the substrate, and polymer/salt complexation.

Directed assembly by chemical modification of the substrate is driven by controlling the interfacial interactions of the block copolymer template and the substrate surface. Although they did not provide examples of directed assembly, Ryu et al.³² and Niemz et al.³³ have each provided examples of modification of solid substrate surfaces for block copolymer nanolithography. Ryu et al. reported the use of a

random copolymer of styrene, methyl methacrylate, and 2 wt % vinylbenzocyclobutene, a reactive cross-linking monomer, to quickly and easily modify solid surfaces without relying on specific surface chemistries. The strength of the interfacial interactions could be modified by controlling the ratio of styrene to methyl methacrylate, whereas the degree of cross-linking could be tuned by changing the amount of cross-linking monomer in the feed. The process was demonstrated on a variety of surfaces including metals, semiconductors, and polymers. Niemz et al. provided an example of similar scope that relies on surface modification using a partial self-assembled monolayer of octadecyltrimethyl chlorosilane. The process is “straight forward and less time consuming, and uses inexpensive commercially available materials,” compared to the neutral-brush approach. Both sets of authors demonstrated the fabrication of well-ordered, nanoporous templates derived from PS-PMMA diblock materials, using their respective surface modification methods. The power of both methods is their generality.

Nealey and co-workers have made significant contributions to the area of directed assembly using chemically nanopatterned surfaces. In 2005, Stoykovich et al. described the directed assembly of ternary PS/PMMA/PS-PMMA polymer film blends into nonregular, device oriented structures.³⁴ The ternary blend consisted of 20 wt % of each homopolymer ($M_n = 40 \text{ kg mol}^{-1}$) and 60 wt % of a symmetric PS-PMMA diblock material with a total number-average molecular weight of 104 kg mol^{-1} . The blend exhibited a lamellar morphology in the bulk state with a periodicity of 70 nm. The chemically patterned substrates were prepared using a four-step process. First, a photoresist was spin-coated onto a PS brush that was grafted to a silicon substrate. The photoresist was then patterned with arrays of lines, straight or bent, using either electron beam or extreme ultraviolet lithography techniques. Third, oxygen plasma etching was used to chemically modify the exposed regions of the PS brush. Finally, the photoresist was removed by solvent rinsing, leaving alternating linear arrays of modified and unmodified PS. Multiple chemically modified surfaces were prepared with different spacings and bending angles between the lines. A film of the ternary blend, approximately 40 nm thick, was spin-coated onto the chemically patterned surfaces, annealed at 193 °C for 7 days, and then analyzed by SEM. As is demonstrated in Figure 9, the PS domain of the ternary blend preferentially wet the unmodified PS brush, whereas the PMMA domain preferentially wet the chemically modified regions, leaving lamellar arrays in remarkable registration with the original modified substrate. It should be noted that the domain dimensions deviate by as much as 10% from those formed in the bulk. Larger deviations cause defects, which are apparent at the corners of the bends. These defects depend on the bend angle and the corner-to-corner lamellar period. Simulations predict the presence of homopolymer-rich material in the middle of the bends of the corners. This patterning method offers the ability to harness the fine control of structure dimensions that block copolymer materials possess and use them for the production of nanoelectronic devices that require patterns more complex than simple periodic arrays. The authors state that this process “may be

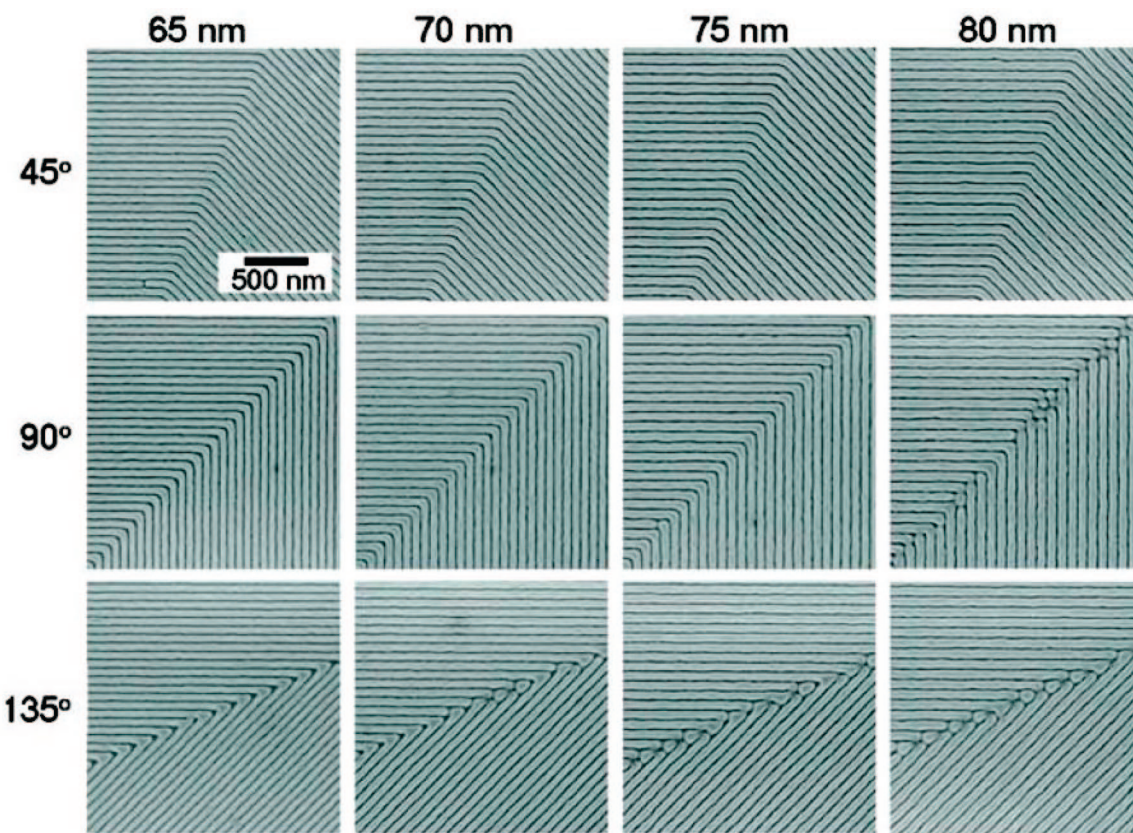


Figure 9. SEM images of a PS-PMMA/PS/PMMA blend directed by chemically modified substrates. Domain periodicities are listed across the top and bending angle along the side. Reprinted with permission from ref 34. Copyright 2005 American Association for the Advancement of Science.

scaled to dimensions of 10 nm and below with precise control over feature size and shape.”

More recently, Park et al. have extended this methodology to pattern cylinder-forming PS-PMMA diblock materials perpendicular to the surface of a chemically modified substrate, which consisted of square arrays of circular spots.³⁵ The methods used to prepare the chemically modified substrates were identical to those described above, with the obvious difference being that square arrays of circular spots were patterned instead of arrays of bent lines. The lattice spacing of the spots were 50–80 nm with diameters of 20–90 nm. Films spin-coated onto unpatterned substrates formed irregularly shaped cylinders oriented perpendicular to the surface, with diameters ranging from 16 to 89 nm and an average intercylinder distance of 88 nm. Films of PS-PMMA spin-coated onto the chemically modified surface were 22–73 nm thick. However, films spin-coated onto chemically patterned substrates exhibited well-aligned square arrays of vertical cylinders. Fast Fourier transform (FFT) analysis of SEM images showed sharp, narrow peaks with a square array. The average cylinder diameter was 45 nm with a total range of 30–52 nm. When the lattice spacing of the chemically patterned substrate was incommensurate with the natural dimension of the PS-PMMA material, surface reconstruction lead to the formation of two micodomain structures that do not appear in the bulk structure (Figure 10). The authors described these morphologies, as “semi-cylinder,” because the cylinder does not completely extend from the top of the film to the substrate, and “loop cylinder,” because a loop structure connects two neighboring cylind-

ders.³⁶ Film thickness was varied to measure its effect on the appearance of these morphologies, as well as overall patterning ability. It was determined that a morphology similar to the bulk morphology occurred when the film thickness was greater than 1.5 times the cylinder microdomain diameter. The authors went on to theoretically probe the exact effect of various dimensional mismatches on the exhibited morphology, but those results are beyond the scope of this work. This report increases the complexity of patternable structures, and demonstrates that the potential of block copolymer lithography can be extended by using chemically patterned surfaces, which are patterned differently from the bulk morphology of the block copolymers. Although these authors did not convert these thin films into nanoporous materials, the PS-PMMA templates they generated are suitable for selective removal of the PMMA component. The previous two patterning methods described by Nealey and co-workers are remarkable examples of the level of control that can be attained.

Li and Huck have investigated physical patterning techniques to form periodic arrays of PS cylinders either normal or parallel to the substrate surface.³⁷ A PS-PMMA diblock copolymer with PS and PMMA number-average molecular weights of 46.1 kg mol⁻¹ and 21.0 kg mol⁻¹ was used for these investigations. The experimental process consisted of four steps (Figure 11). First, a silicon surface was neutralized by thermally anchoring a 5 nm thick layer of random PS-PMMA copolymer to the native silicon oxide layer. The PS-PMMA diblock copolymer described above was then spin-coated onto the neutralized surface from toluene. Diblock

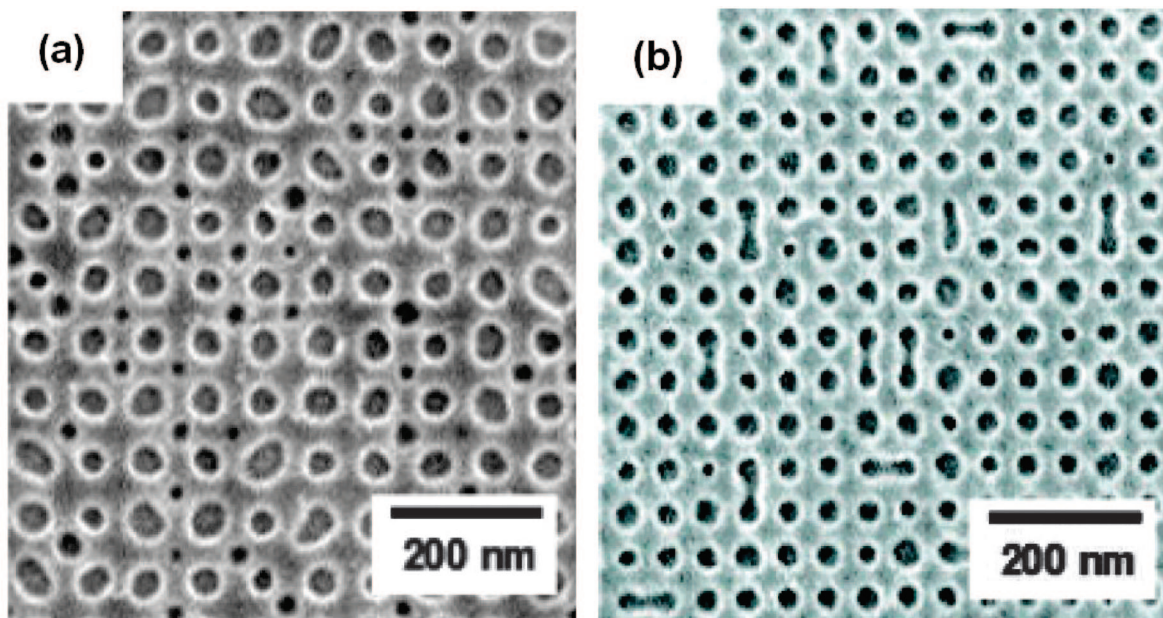


Figure 10. SEM images of PS-PMMA thin films on chemically patterned substrates demonstrating (a) semicylinder and (b) loop cylinder morphologies. Reprinted with permission from ref 35. Copyright 2007 American Chemical Society.

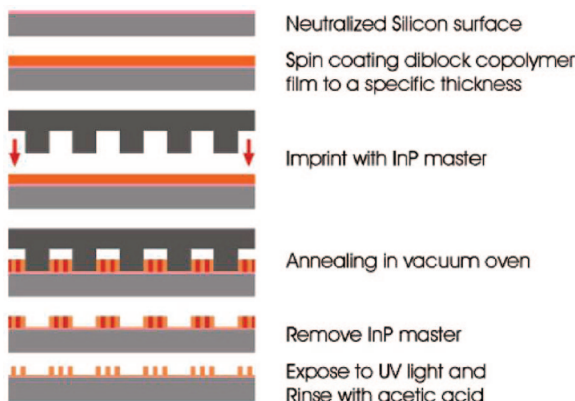


Figure 11. Preparation of nanoimprint lithography PS-PMMA block copolymer self-assembled patterns. Reprinted with permission from ref 37. Copyright 2004 American Chemical Society.

film thicknesses ranged from 25 to 45 nm as measured by ellipsometry. Next, a nanoimprint lithography mold was pressed against the surface of the diblock copolymer film at pressures up to 5 MPa and the samples were annealed at 180 °C for 20 h, with the mold still in place. Molds had either a 200 or 210 nm periodicity and a 100 or 120 nm spacing with a channel depth of 135 nm. Finally, the PMMA was selectively etched using the standard UV/acetic acid procedure. The block copolymer film thickness was 25 nm in both cases, and the cylinders are clearly aligned normal to the surface. When similar techniques were used on block copolymer films with a thickness of 45 nm, aligned cylinders were again achieved, although they were oriented parallel to the substrate. Although alignment has not yet been optimized, the experimental simplicity of this method makes it very appealing for future nanodevice fabrication.

Xiao et al. reported using physically patterned substrates to align cylinder-forming PS-PMMA.³⁸ Topographic patterns of alternating grooves and ridges on a silicon substrate with a depth of 50 nm and width 150–600 nm were first

neutralized with hydroxyl-terminated PS-*r*-PMMA random copolymer, followed by spin-coating of a 1% (w/w) PS-PMMA toluene solution. Surface neutralization circumvented the problem of a wetting layer of block copolymer at the vertical interface; the presence of such a layer could cause irregular pattern transfer. SEM images revealed an ordered cylindrical morphology of PS-PMMA in patterned domains, perpendicular to the bottoms of the grooves. The formation of half-cylinders at the neutral sidewalls confirmed the absence of a wetting layer. Moreover, the number of rows of cylinders was well-controlled by the groove width. PMMA removal led to nanoporous templates with uniform size and spacing. These templates are potentially very useful for producing high-performance magnetic metal nanoarrays.

Finally, polymer/salt complexation methods have been investigated for directed assembly. Kim et al. explored the effect of ion complexation on the nanodomain ordering in a cylindrical PS-PEO thin film.³⁹ Solvent annealing of spin-coated PS-PEO thin films promote long-range lateral order with cylindrical nanodomains aligned normal to the substrate. In this work, different amounts of KI were intentionally added to a PS-PEO copolymer solution. The complexation of KI with the PEO block was examined by IR spectroscopy, showing a slight shift of the C—O—C stretching peak. For this specific PS-PEO sample, without any salt, parallel orientation of PEO cylinders in thin films was obtained. With small to medium amounts of added salts, highly ordered arrays of hexagonally packed cylindrical microdomains oriented normal to the surface were produced. The authors suggest that the complexation of the salt and PEO eliminates the preferred interaction between the substrate and the PEO block. The lateral ordering was markedly improved because of the increased segregation strength between the two blocks along with the enhanced mobility of the polymer chains. Additionally, the authors demonstrated that using other PEO selective salt complexes, such as HAuCl₄, produced Au

nanostructures in confined PEO domains. This strategy can be potentially extended to other copolymer systems as a facile way to control film orientation, and these systems could be particularly well suited for the formation of highly ordered nanoporous templates.

More recently, Li et al. published work in which they also produced Au nanoparticles confined in a polymer domain.⁴⁰ A polystyrene-*b*-poly(2-vinylpyridine) (PS-P2VP) diblock with PS and P2VP number-average molecular weights of 54.9 and 18.6 kg mol⁻¹, respectively, was blended with PMMA ($M_w = 23.6$ kg mol⁻¹) and HAuCl₄. Polymer films were produced by spin-coating the mixture onto silicon (with native oxide layer), SiO₂, and gold substrates. The chloroauric acid forms a complex with the pyridine units in the block copolymer, which adjusts the interaction between P2VP and the substrate surface. Hexagonally packed cylindrical morphologies oriented normal to the substrates surface were obtained, with the addition of HAuCl₄ markedly enhancing the perpendicular orientation. The films were then exposed to deep UV irradiation to simultaneously degrade the PMMA and reduce the HAuCl₄ to Au. Following an acetic acid rinse, the top and bottom of the etched film were investigated by AFM, confirming that pores extended completely through the sample. Finally, XPS measurements confirmed the presence of atomic Au. This methodology could prove to be very beneficial for the fabrication of hybrid-metal-containing nanostructures.

3. Monolithic Materials

Discussion of the nanoporous materials described above was focused on thin film block copolymer templates for nanolithographic applications. However, a variety of other applications exist where monolithic (or macroscopic) nanoporous materials would be desirable. Current examples of such applications include mesoporous silica monoliths for optical and separations applications,⁴¹ macroporous polymer monoliths for chromatographic separations,⁴² and monolithic catalysts for industrial applications.⁴³ Multiple examples of the design and preparation of nanoporous polymeric templates have been reported. Subsequent efforts have focused on designing and controlling the pore wall functionality, with several examples of their preparation and application being recently disclosed.

Rzayev and Hillmyer published work on the formation of nanoporous polystyrene-containing hydrophilic pores via the selective degradation of PLA in a polylactide-*b*-poly(*N,N*-dimethylacrylamide)-*b*-polystyrene (PLA-PDMA-PS) tri-block terpolymer.⁴⁴ This tri-block material was prepared using a combination of controlled ring-opening and free-radical polymerization techniques. First, PLA was synthesized by controlled ring-opening polymerization followed by end-capping with a trithiocarbonate moiety. This moiety was subsequently used to consecutively grow PDMA and PS blocks by RAFT polymerization. The final PLA-PDMA-PS material had a number-average molecular weight of 46 kg mol⁻¹ and PDI of 1.12 by SEC. The overall weight fraction of PLA was 0.25 and the material formed hexagonally packed PLA cylinders in a PS matrix with the short PDMA

blocks localized at the PS-PLA interface. A channel die aligned sample of this material was subjected to a water/methanol solution of NaOH above the glass transition temperature (T_g) of PLA, but below the T_g of PDMA and PS. Complete removal of the PLA was demonstrated by NMR spectroscopy and SEC. SAXS and SEM were used to confirm the porosity of the resulting material. Degradation of the PLA left the pores of the material lined with the hydrophilic PDMA component. The hydrophilic nature of these pores was confirmed by a simple experiment of placing the monolithic sample in water. After a few minutes, the sample sank to the bottom of the vessel, indicating efficient water uptake. In contrast, similar materials obtained from PS-PLA diblock copolymer materials remained on the surface of the water for several months. Water uptake was further quantified by TGA and differential scanning calorimetry of the water laden monoliths. This publication is significant in the fact that it established that monolithic samples of nanoporous polystyrene can be prepared with hydrophilic pores that render the materials water-compatible.

In a full paper, following their 2005 communication, Rzayev and Hillmyer described the tailoring and further modification of the PDMA lined pores.⁴⁵ Ten different PLA-PDMA-PS samples with PDMA volume fractions ranging from 0.04 to 0.27 and PLA volume fractions ranging from 0.15 to 0.30 were prepared. Monolithic samples were aligned and degraded as previously discussed. Interestingly, the rate of degradation of the PLA was found to depend on the size of the PDMA block, with short PDMA chain samples degrading more rapidly. The authors noted that this observation suggests a “transport-limited mode” of degradation of the PLA within the sample. Nanoporous structures were characterized by SAXS and SEM. Samples demonstrated high degrees of alignment with second-order orientation factors values ranging from 0.92 to 0.96. Figure 12 shows images, with total area of approximately 1 μm^2 , of the nanoporous monoliths and clearly demonstrate the remarkable long-range order that results from alignment. The thickness of the internal PDMA lining in the pores of the PS-PDMA monoliths could be controlled by varying the triblock terpolymer composition. Materials with PDMA thickness from 0.8 to 3.5 nm (by SEM) were prepared, effectively varying the functional group density at the interior surface.

The hydrolysis and further functionalization of the internal PDMA coating was extensively investigated. Although the PDMA was extremely stable under basic conditions, when the same materials were subjected to an acidic environment, the amide groups readily hydrolyzed to provide carboxylic acid functionalities on the pore walls. Although complete conversion of PDMA to poly(acrylic acid) (PAA) was achieved after 2 days, shorter reaction times yielded partially hydrolyzed samples. Thus, nanoporous monoliths with a range of properties, from completely neutral and hydrophilic to highly charged, could be prepared from a single block copolymer precursor. The PAA lining also provided a reactive coating on the internal pore surface that allowed for further functionalization of the pore walls. Carbodiimide mediated couplings of amines and carboxylic acids were investigated. Additionally, nanoporous PS-PAA monoliths

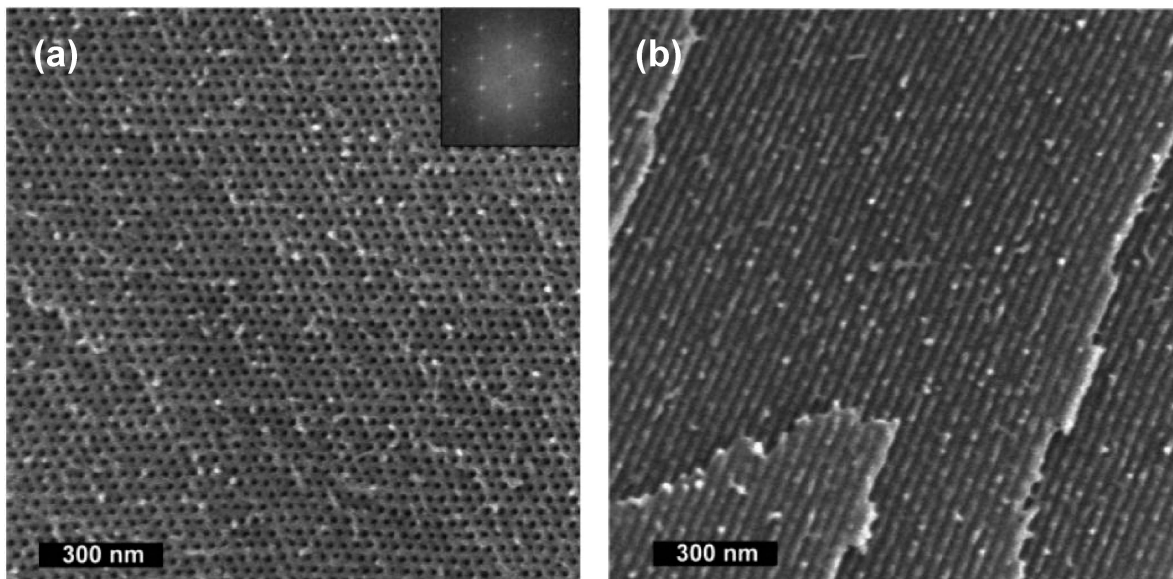


Figure 12. SEM images of nanoporous PS-PDMA materials (a) perpendicular and (b) parallel to the direction of pore alignment. Reprinted with permission from ref 45. Copyright 2005 American Chemical Society.

were reacted with a variety of amines, which incorporated different functional groups such as pyridine, a chiral hydroxyl, and an alkene, into the nanoporous structure. This work established the feasibility of an extraordinarily powerful and versatile modification route that allowed for control over the interior surface properties of the resulting nanoporous monoliths that has not been rivaled in the literature today.

Other routes toward the preparation of functionalized nanoporous materials using the general triblock-terpolymer-based approach have also been reported. For example, Bailey et al. investigated the use of alkene groups in PS-PI-PLA triblock terpolymers as latent reactive sights for subsequent modification of the nanoporous monolith.⁴⁶ Eighteen triblock terpolymers with PLA volume fractions between 0.19 and 0.40 and PLA molecular weights of 3.5 to 24.4 kg mol⁻¹ were prepared using a combination of anionic and controlled ring-opening polymerization techniques. The morphologies of the resulting materials were characterized by SAXS; a majority of the samples exhibited a hexagonally packed cylindrical morphology. TEM, used to directly image the materials, confirmed a core–shell geometry of the cylindrical domains for samples exhibiting the targeted hexagonal symmetry (Figure 13). Channel die alignment procedures similar to those previously described were investigated. The overall molecular weight of the materials was found to have a dramatic effect on the degree of alignment, with the highest-molecular-weight materials demonstrating a significant kinetic resistance to ordering.

Selective degradation of the PLA block of the PS-PI-PLA triblock materials proved to be more difficult compared to the other PLA containing materials described above. A small-scale screening was performed using several different bases with a variety of organic additives at different concentrations, all at different temperatures and for varying amounts of time, to find a set of usable etching conditions. This combinatorial effort demonstrated that 95–100% PLA degradation occurred with an aqueous solution of 0.1 wt % sodium dodecyl sulfate in 0.5 M NaOH at 50 °C for 7–10 days. However, similar

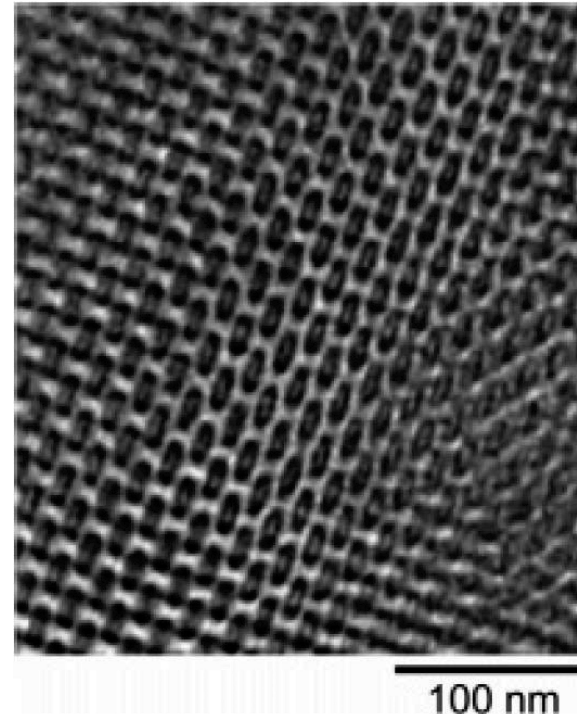


Figure 13. TEM micrograph of a PS-PI-PLA monolith possessing a core–shell geometry of hexagonally packed PLA cylinders surrounded by a PI shell in a matrix of PS. (PI domains have been stained with OsO₄.) Reprinted with permission from ref 46. Copyright 2006 American Chemical Society.

to the case with alignment, the molecular weight of the materials played a major role in the extent of degradation. Low- (17.5 kg mol⁻¹) and high- (46.8 kg mol⁻¹) molecular weight samples of identical composition showed considerable resistance to PLA degradation. The authors suggest that low-molecular-weight materials showed resistance to degradation because of pore collapse or surface rearrangement, whereas lack of long-range order in the high-molecular-weight materials was implicated.

In contrast to the low and high molecular weight materials, intermediate molecular weight materials yielded clean, quantitative PLA degradation with high degrees of alignment. The resulting nanoporous PS-PI monoliths had pore walls lined with alkene functional groups from the PI block. These inherently reactive functional groups were used to further modify the interior of the pore walls through epoxidation. Epoxidation was chosen because of its potential use as a latent coupling agent for the generation of more sophisticated support frameworks. Two sets of epoxidation conditions were investigated: peroxyacetic acid in acetic acid/water solution and *m*-chloroperoxybenzoic acid (MCPBA) in *tert*-butyl alcohol/water solution. Although the peroxyacetic acid route was plagued with the side reaction of acid-catalyzed opening of the resulting epoxide ring, the MCPBA reaction cleanly yielded an epoxide functionalized nanoporous PS-PI material. Approximately 75% conversion of the PI alkene units was achieved after reaction for three days, as measured by NMR spectroscopy. SAXS and SEM showed that the nanoporous PS-PI structure was maintained following epoxidation, although a moderate loss of alignment was observed. Despite this loss of alignment, these materials still serve as excellent examples of materials that could be used to fabricate more complex nanoporous structures.

The previous monolithic examples employed PLA as the etchable component. In 2005, Mao and Hillmyer demonstrated a procedure using PEO as an etchable block to generate nanoporous materials from PS-PEO diblock copolymers.⁴⁷ Given the wide number of PEO-containing block copolymers available today, this strategy could prove to be a very powerful method for fabricating nanoporous materials. Diblock materials with a PS molecular weight of 27 kg mol⁻¹, PEO molecular weight of 13 kg mol⁻¹, and overall PDI of 1.04 were prepared by sequential anionic polymerization. Following channel die alignment, SAXS analysis was used to determine that the sample exhibited a cylindrical morphology, with PEO cylinders 17 nm in diameter in a PS matrix. The monolithic sample was then immersed in 57 wt % aqueous HI solution at 60 °C. After 5 days, NMR spectroscopy and SEC data were consistent with complete removal of PEO from the sample. Pore size of the degraded material was 15 nm (by SEM), consistent with the pore size of the original diblock material.

Mao and Hillmyer expanded this method of using PEO as an etchable block in a subsequent 2005 publication.⁴⁸ The expansion was 2-fold: targeting a bicontinuous gyroid morphology instead of a cylindrical one and taking advantage of the hydrophilic nature of PEO to prepare nanoporous materials that were water wettable. PS-PLA and PS-PEO diblock materials were prepared by anionic polymerization. The PS-PLA diblock had a total molecular weight of 21.1 kg mol⁻¹ with a PS volume fraction of 0.58, and the PS-PEO diblock had an overall molecular weight of 30.5 kg mol⁻¹ with a PS volume fraction of 0.63. SAXS analysis of the diblock materials showed that the PS-PLA material was lamellar while the PS-PEO material was cylindrical. However, order–order transitions of both materials were observed in dynamic mechanical analysis. The PS-PLA sample underwent a lamellar to gyroid transition at 211 °C, whereas

the PS-PEO sample underwent a cylindrical to gyroid transition at 208 °C. The gyroid morphology in both samples persisted upon cooling the samples below the T_g of PS. Subsequently, it was demonstrated that the order–order transition in both samples could be induced by simply heating the materials at 200 °C overnight followed by quenching to room temperature. Both samples were degraded using aqueous HI as described above. SEM images of a fractured surface of the respective monoliths confirmed the nanoporosity and ordered state symmetry of the materials. Additionally, the porosity of the PS-PLA derived nanoporous materials was investigated using nitrogen adsorption experiments. The nanoporous materials exhibited a type IV isotherm with an H1 type hysteresis, properties characteristic of mesoporous materials with a narrow pore size distribution. Barrett–Joyner–Halenda (BJH) analysis of the data gave average pore diameters of 11.8 and 12.2 nm for the PS-PLA and PS-PEO derived nanoporous materials. Both of these values were consistent with SEM and SAXS analysis.

Finally, a strategy of blending the two diblocks was investigated in an attempt to prepare water wettable nanoporous materials. Using the same synthetic techniques, a second PS-PEO sample with an overall molecular weight of 19.5 kg mol⁻¹ and volume fraction of PS of 0.61 was prepared. A miscible blend of 11 wt % PS-PLA and 89 wt % of the second PS-PEO sample was prepared, annealed overnight at 200 °C, and quenched to room temperature. As with the diblock materials, the blended material exhibited a gyroid morphology (as determined by SAXS). The blended sample was degraded in aqueous NaOH to selectively etch the PLA block, leaving the PEO block untouched. NMR analysis confirmed complete degradation of the PLA with little change in the PEO composition. SAXS and SEM data again confirmed retention of the gyroid pore structure after degradation. Unlike the previous PS-PEO and PS-PLA materials, this blended nanoporous material proved to be completely water wettable. When placed in a vial of water, the blended nanoporous sample filled with water and became fully submerged after 71 h at room temperature; the neat samples floated on the surface.

Another interesting continuous nanoporous network possessing a bicontinuous gyroid morphology was presented by Okumura et al. in 2006.⁴⁹ A blend of P2VP-PI and PI, with a P2VP volume fraction of 0.34, was first treated with 1,4-diiodobutane to cross-link the P2VP domain. The cross-linking was followed by selective degradation of the PI matrix by ozonolysis. FESEM images of free-standing nanoporous gyroid structures were obtained, which were in good agreement with 3-D computer simulations. In a following publication by Hashimoto et al., more detailed analysis of FESEM images was undertaken for two nanoporous gyroid blended samples: the P2PV-PI/PI blend discussed above and a PS-PI/PS blend with a PI volume fraction of 0.34.⁵⁰ Numerical analyses at different cross-sections in 3-D space were performed, and corresponded well with results directly observed by FESEM. Both examples demonstrated the fabrication of gyroid nanoporous films, which are of great interest for future applications.

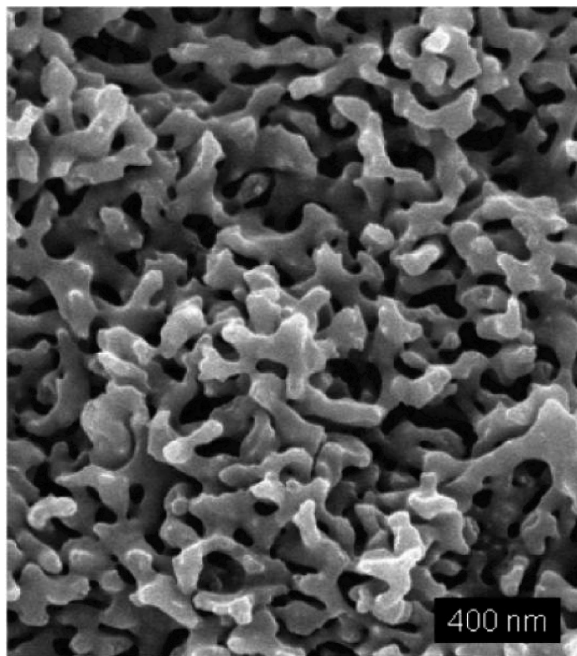


Figure 14. SEM image of nanoporous material templated from a PI/PS/PS-PI bicontinuous microemulsion. Reprinted with permission from ref 51. Copyright 2006 American Chemical Society.

In 2006, Zhou et al. reported the preparation of a nanoporous material with a bicontinuous morphology by a novel method utilizing the bicontinuous microemulsion formed by blending a diblock copolymer with its corresponding homopolymers.⁵¹ The nanoporous material prepared by Zhou et al. was derived from a polymeric bicontinuous microemulsion precursor.⁵² The bicontinuous microemulsion was prepared by blending PI, PS, and a symmetric PI-PS diblock copolymer with molecular weights of 3.1, 3.4, and 16 kg mol⁻¹, respectively. The composition window of the bicontinuous microemulsion phase was located using a combination of SAXS, rheology, and optical microscopy along the isopleth where the two homopolymers were mixed in equal volumes. Blends were prepared by codissolution of the three polymeric materials in benzene followed by vacuum-drying to constant weight. The bulk bicontinuous microemulsion samples were annealed at 100 °C for 10 min, followed by rapid cooling to room temperature to vitrify the PS phase. Sulfur monochlorite vapor was used to cross-link the continuous PI phase. After exposure for 2 weeks, the samples turned brown in color. Following cross-linking, the PS homopolymer was removed by dissolution in hexane, leaving the PS block from the PS-PI diblock copolymer lining the pore walls. FTIR spectroscopy indicated no residual double bonds from PI. SEM images of freeze-fractured specimens of the samples shown in Figure 14 demonstrate a broad interconnected pore network. The nanoporous materials showed reasonable thermal stability, remaining intact even after heating to 200 °C. Because the materials were cross-linked, they also demonstrated reasonable solvent resistance; they were completely insoluble in benzene, acetone, and THF. When submerged in the ionic liquid butyl methyl imidazolium phosphorus hexafluoride, the samples sank to the bottom of the flask after several

hours. This sinking indicated substantial solvent uptake, even though the pores were lined with PS, which was not soluble in the ionic liquid. Electrical conductivity of the filled structures measured by AC impedance spectroscopy was 3.89×10^{-4} S cm⁻¹ at room temperature. This value compares to a conductivity of 1.4×10^{-3} S cm⁻¹ for the neat ionic liquid. These conductivity results confirmed that most of the original PS nanodomains percolated through the bicontinuous microemulsion. The overall porosity of the material was approximately 0.45, so a tortuosity factor of 2 could be inferred for these membrane materials. Finally, BET methods were used to probe the porous nature of the materials, with BJH analysis giving a most probable pore diameter of 43 nm. Significantly, the pore sizes accessible by this procedure are substantially larger than those typically achievable using pure block copolymers, and the bicontinuous structure eliminates the need for external alignment.

Aligned monolithic materials such as the ones described above have opened new avenues for the investigation of fundamental physical phenomena such as nanocrystal growth and evaluation. For example, Ha et al. used nanoporous monolithic PS materials derived from PS-PLA templates, prepared as described above, to investigate the properties of organic nanocrystals embedded in polymeric nanoporous materials.⁵³ The crystallization and melting behavior of two different organic compounds, 2,2,3,3,4,4-hexafluoro-1,5-pentanediol (HFPD) and (R)-(+)-3-methyladipic acid (R-MAA), were investigated in nanoporous PS and nanoporous controlled pore glass. The confined HFPD and R-MAA nanocrystals were generated by either evaporation of methanol solutions or cooling of a melt that had been imbibed into the porous structure of the nanoporous materials. The formation of nanocrystals was confirmed by X-ray microdiffraction, which also allowed for the characterization of the size of the nanocrystals. Regardless of the nanoporous material, the melting behavior of the organic nanocrystals was shown to be strongly influenced by the channel diameter, with melting point depression scaling inversely with crystal size. More importantly, the melting behavior of the nanocrystals was influenced by the matrix material, with the PS matrix exerting a more pronounced effect on the melting point depression and enthalpy of fusion. Specifically for the case of HFPD, the X-ray microdiffraction data revealed a preferred orientation for the nanocrystals embedded in the PS matrix. The authors suggested that this orientation is caused by favorable wetting of the pore walls by certain crystal planes. Finally, the authors used this collection of results to argue that assumptions used previously to describe the thermotropic properties of organic nanocrystals “do not capture all the terms necessary to characterize the behavior associated with the nanoscale dimensions of the crystals and their interactions with the channel walls of the embedding materials.”

4. New Techniques for Preparing Nanoporous Materials

Several new techniques have been recently developed for the preparation of nanoporous materials. These techniques

can broadly be divided into three areas: the development of organic nanostructures with enhanced thermal and mechanical properties, the investigation of new fabrication or etching techniques, and the use of organic block copolymers for the preparation of inorganic nanostructures. This section will detail these three areas of research.

Nanoporous polymeric materials have several advantages over traditional nanoporous inorganic materials, including tunable pore size and the ability to easily incorporate pore functionality. However, many of these polymeric materials possess poor mechanical and thermal properties. For example, PS, the most widely studied polymeric nanoporous material, is a brittle thermoplastic with a comparatively low T_g . Novel cross-linked nanoporous PS thin films were prepared by Drockenmuller et al. in 2005 to improve the thermal and mechanical performance of the resulting nanoporous materials.⁵⁴ A new functional block copolymer, poly(vinylbenzylcyclobutene-*r*-styrene)-*b*-polymethylmethacrylate (P(BCB-*r*-S)-PMMA), was synthesized by controlled free-radical copolymerization of vinylbenzylcyclobutene with styrene followed by the sequential addition of methyl methacrylate. This material is unique in that it incorporates thermally cross-linkable units on the polymer backbone. Spin-coating P(BCB-*r*-S)-*b*-PMMA on a silica substrate followed by annealing at elevated temperatures yielded a cross-linked nanostructured film. Differential scanning calorimetry of the film before cross-linking showed two distinct T_g values and a strong exothermic peak (due to cross-linking). Upon cross-linking, a single T_g was evident at 130 °C. After UV-etching of the PMMA block, the authors obtained hexagonally packed and lamellar nanoporous thin films. The nanoporous materials were thermally stable up to 150 °C and resistant to good solvents such as toluene. This cross-linking strategy resulted in the pronounced enhancement of the thermal and mechanical stability of the nanoporous materials compared to standard nanoporous PS materials.

In follow up work pursuing the same cross-linking strategy, P(BCB-*r*-S)-PLA copolymers were used to prepare cross-linked nanoporous PS films by etching the PLA block under basic conditions.⁵⁵ The cross-linked nanoporous films were shown to be stable up to 200 °C. More importantly, hydroxyl functionality inside the nanopores could potentially provide a facile route to chemical functionalities in the thin film templates, even at elevated temperatures.

More recently, Guo et al. prepared a series of cross-linked nanoporous poly(1,2-butadiene) (PB) materials from a poly(1,2-butadiene)-*b*-poly(dimethylsiloxane) (PB-PDMS) diblock copolymer precursor, to investigate the affect of degree of cross-linking on nanoporous structure.⁵⁶ The PB-PDMS material had a number-average molecular weight of 15.0 kg mol⁻¹, PDI of 1.22, and volume fraction of PDMS of 0.29. Following the synthesis of the parent PB-PDMS material, a series of eight cross-linked samples were prepared using dicumyl peroxide as a cross-linking initiator at 140 °C under an argon atmosphere. FTIR was used to quantify the concentration of double bonds in the samples after cross-linking relative to the parent diblock. The fraction of consumed double bonds varied from 11 to 89% throughout the eight samples. Swelling ratios of the cross-linked diblocks were

also investigated and used in conjunction with the Flory model to determine the degree of polymerization between cross-links. The relationship between the fraction of consumed double bonds and the inverse of degree of polymerization between cross-links was approximately linear.

Cross-linked diblock materials were then immersed in 1.0 M tetrabutylammonium fluoride to selectively etch the PDMS block. Etching was confirmed by FTIR. In a separate experiment, the parent diblock material was subjected to the same etching conditions, and NMR spectroscopy was used to confirm that no double bonds were lost during the etching protocol. The etched samples were characterized by SAXS and methanol uptake studies. Three classifications of etched materials were created on the basis of these results: collapsed, “traced”, and nanoporous. Collapsed materials exhibited no principle scattering peak in SAXS and no appreciable methanol uptake. Traced materials demonstrated a slight increase in intensity of the principle SAXS scattering peak, compared to the neat sample, and had approximately 20 wt % methanol uptake after 150 h. Nanoporous materials showed a large increase (several orders of magnitude) in the intensity of the principle SAXS scattering peak, compared to the neat sample, and had methanol uptakes equal to the weight fraction of PDMS in the parent polymer after only 2 h. This work provides important information for the development of cross-linked nanoporous materials.

Although cross-linking methods have been shown to be useful to attain enhanced thermal and mechanical stability, the use of mechanically robust matrix materials has been investigated. In 2006, Uehara et al. reported the preparation of semicrystalline nanoporous polyethylene (PE) films from polyethylene-*b*-polystyrene (PE-PS) precursors. The resulting films showed significant mechanical strength (Figure 15).⁵⁷ Self-assembly of the PE-PS was governed not only by the melt-phase thermodynamics, but also by crystalline-induced segregation. Experimentally, copolymers were annealed at 180 °C and then isothermal crystallization of the PE block was induced at different temperatures between 70 and 90 °C. The resulting morphologies of the films were characterized by TEM. The results revealed that the isothermal crystallization temperature was crucial (preferably at 90 °C) for formation of a bicontinuous morphology. The amorphous PS domains were subsequently chemically etched with fuming nitric acid. The resulting bicontinuous nanoporous PE membrane had a surface area of 17 m² g⁻¹ by BET analysis, and excellent mechanical strength. More importantly, the gas permeation rate of this membrane was 1.4 times that of a commercially available porous polyolefin membrane. This work is the first reported example of a highly flexible nanoporous material, and could find utility in a variety of membrane applications.

The second area of focus for the production of novel nanoporous materials has been the development of innovative fabrication techniques. In 2004, Yokoyama and co-workers successfully demonstrated the facile fabrication of uniform nanocells in polystyrene-*b*-poly(perfluoroctylethyl methacrylate) (PS-PFMA) diblock materials using supercritical CO₂ (scCO₂) as a porogenic reagent, where the PFMA serves as a CO₂-philic block.^{58,59} Films of the PS-PFMA material,

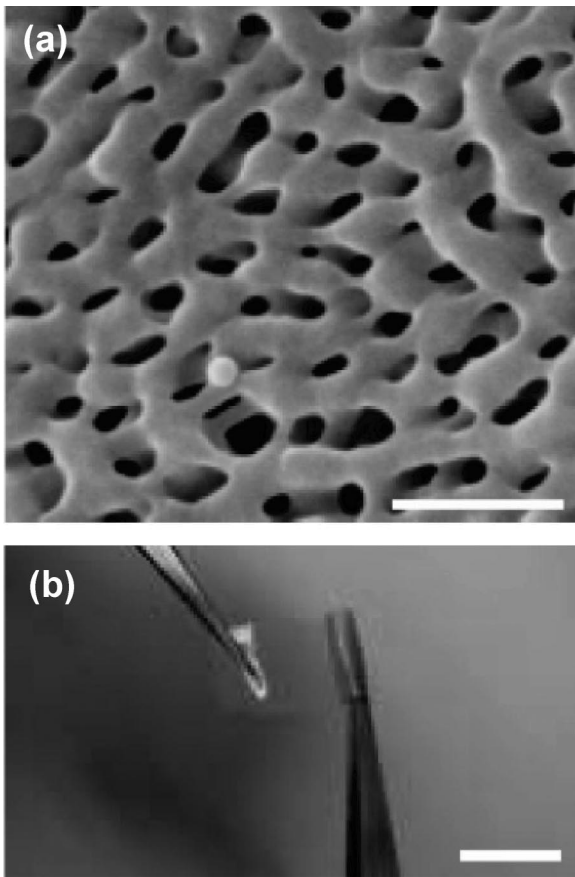


Figure 15. Images of semicrystalline nanoporous PE films: (a) SEM and (b) photograph of rolled film. (the scale bars represent 200 nm and 10 mm, respectively). Reprinted with permission from ref 57. Copyright 2006 American Chemical Society.

100 μm thick, were placed in a high-pressure vessel, with CO_2 at a pressure of 7.5–30 MPa at 60 $^\circ\text{C}$ for 1 h. The temperature was reduced, over 10 min, to 0 $^\circ\text{C}$ under constant pressure. Finally, the CO_2 pressure was released at a rate of 0.5 MPa min^{-1} . The resulting structures were investigated by SAXS and SEM. Average diameters of the cellular networks were 10–30 nm, depending on the CO_2 pressure. In two subsequent full papers, Yokoyama and co-workers addressed the ability to control pore size and distribution (Figure 16).^{60,61} First, a depressurization temperature (T_d) lower than the T_g of the CO_2 -swollen PS block was critical in the formation of nanocells. As the T_d approached the T_g of the CO_2 -swollen PS, a coexistence of nanocells and microcells was obtained. The authors argued that the two different cell sizes were developed by two independent processes. Nanocells were formed at a low T_d , where the fluorinated block nucleated nanobubbles of CO_2 . Microcells were formed at a high T_d from CO_2 in the PS matrix, similar to the conventional CO_2 foaming process of PS. (Presumably the lower T_d provided a more rigid PS matrix, which forced nucleation over expansion). Furthermore, the nanocells had a maximum diameter of approximately 40 nm. This limit is apparently determined by the balance between the expansion of the nanocells and the diffusion of CO_2 , either into the growing microcells or to the surface to evaporate. This work demonstrated the production of tunable spherical pores, from

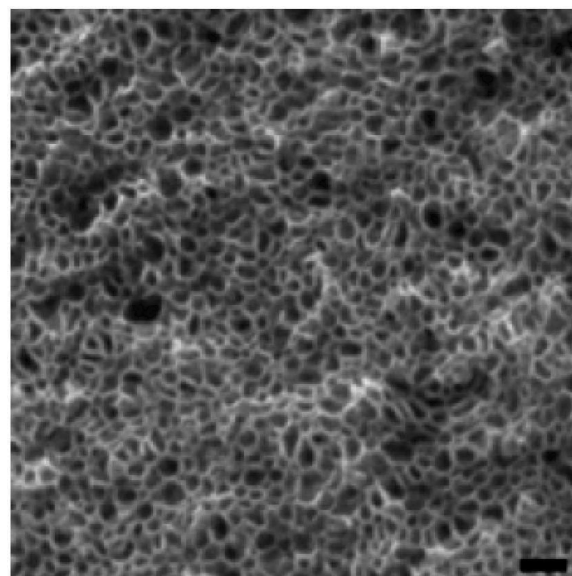


Figure 16. SEM image of a nanocellular PS monolith. The sample was pressurized to 30 MPa at 60 $^\circ\text{C}$ and depressurized at 25 $^\circ\text{C}$ at a rate of 0.5 MPa min^{-1} (the scale bar represents 200 nm). Reprinted with permission from ref 60. Copyright 2006 American Chemical Society.

microcells to nanocells, without chemical degradation of any of the constituent blocks.

Supramolecular strategies have also been investigated as new fabrication techniques. These strategies are advantageous because the etching step typically consists of removing only a small molecule or breaking a single bond joining the blocks of a block copolymer. Laforgue et al. studied the self-assembly of polystyrene-*b*-poly(4-vinylpyrrolidone) (PS-P4VP), composed of 30 wt % P4VP, mixed with 1,5-dihydroxynaphthalene (DHN).⁶² The DHN selectively enriches the P4VP domains, forming hydrogen-bond complexes with the lone pair of electrons along the P4VP backbone. Thin films of the mixture were prepared on a silicon substrate (with native oxide layer) by dip-coating from tetrahydrofuran (THF). AFM and TEM indicated the morphology consisted of hexagonally packed P4VP/DHN cylinders, oriented normal to the substrate, embedded in a PS matrix. The effect of the DHN:4VP (i.e., OH:N) molar ratio on the diameter of the P4VP/DHN cylinders was investigated. Cylinders approximately 22 nm in diameter resulted from a stoichiometric balance of DHN and 4VP. As this balance was tipped to the side of excess DHN, cylinder diameters increased to over 30 nm with nearest-neighbor distance increasing to approximately 65 nm. Nanoporous films were readily obtained by selective removal of DHN from the P4VP domains via dissolution in methanol.

A second supramolecular strategy developed by Fustin et al. utilized a reversible linkage at the juncture of the two blocks of a diblock copolymer for the fabrication of nanoporous thin films.⁶³ The novel element of this approach was the use of a ruthenium(II)-terpyridine bis-complex ([Ru]) to tether a PS and PEO block, thus forming a PS-[Ru]-PEO diblock copolymer. Thin films of the diblock complex formed from spin-coating onto a silicon substrate formed a cylindrical morphology with the cylinders oriented normal to the surface. The average cylinder diameter was 33 nm. Following

a “brief” exposure under UV light at an intensity of 3 J cm^{-1} to cross-link the PS, the film was reduced in a 0.01 M aqueous $\text{Ce}(\text{SO}_4)_2$ solution for 30 min. This procedure simultaneously “opened” the [Ru] complex and dissolved the free PEO chains. PEO removal was verified by XPS. Cylinder diameter after PEO removal was in agreement with the diameter of the cylinders prior to reduction.

Zhang et al. used a very similar strategy to prepare nanoporous films from PS-PEO diblock materials.⁶⁴ The PS-PEO materials investigated contained a cleavable juncture, a triphenylmethoxy (trityl) ether linkage, between the two blocks. The diblock used had number-average molecular weights of 19.6 kg mol^{-1} and 5.0 kg mol^{-1} for the PS and PEO blocks, respectively. Native diblock samples as well as a sample with a KI salt additive for improved lateral order (following the methodology described previously in this work³⁹) were spin-coated onto cleaned silicon substrates. Following benzene solvent annealing, the samples demonstrated a cylindrical morphology with a principle spacing of 21 nm. A variety of etching conditions were investigated. Trifluoroacetic acid (TFA) vapor readily induced cleavage of the trityl ether linkage in the native film and the detached PEO homopolymer chains migrated to the film surface, as evidenced by the formation of PEO crystals on the film surface. However, the “salted” film did not produce efficient cleavage under the same conditions. The authors suggested that a pseudocrown ether complex between PEO and KI retarded cleavage. Immersing the salted sample in a water/methanol mixture disrupted these interactions, allowing for efficient cleavage. Finally, direct immersion of the films in TFA or HCl in a water/methanol mixture also produced efficient cleavage. Examination of the nanoporous films by TEM showed that lateral order and principal spacing was maintained after etching for all samples. The power of both to these two previous strategies is the efficiency of the etching step, where only the bond between the two blocks is broken. We believe this represents an important advance to the field and anticipate further exploitation of these strategies.

The last area of focus for novel nanoporous synthetic techniques has been the preparation of nanoporous inorganic structures. The critical development has been the incorporation of an inorganic precursor block, which can be hydrolyzed or pyrolyzed to form an inorganic structure, directly in the block copolymer. This strategy allows for the potential fabrication of complex inorganic nanostructures. Li and Yokoyama employed the scCO₂ swelling process described above⁶⁰ to introduce porosity into a PS-PDMS diblock copolymer system, where the PDMS block was selective for CO₂.⁶⁵ This nanoporous film was then oxidized by exposure to UV light/ozone to convert the PDMS into silica. Silica “nanocapsules” were formed, with a diameter less than 40 nm and wall thickness of 2 nm. These nanocapsules were subsequently exposed to controlled RIE conditions to remove the top half of the capsule, forming the “nanocaldrons” shown in Figure 17. Fabrication of these types of inorganic nanostructures is very impressive, and is nearly impossible using conventional techniques.

Another example of the fabrication of complex inorganic nanostructures has been demonstrated recently by Rider et

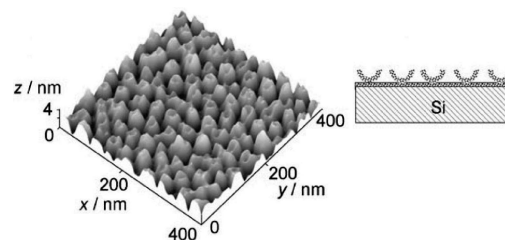


Figure 17. Three-dimensional AFM topographic image of etched hollow silica particles and schematic picture of nanocaldron topography. Reprinted with permission from ref 65. Copyright 2006 Wiley-VCH Verlag GmbH & Co. KGaA.

al.⁶⁶ Polystyrene-*b*-polyferrocenylsilane (PS-PFES) diblock materials were synthesized by sequential anionic polymerization.⁶⁷ Two PS-PFES materials, having total number-average molecular weights of 38.7 and 68.2 kg mol^{-1} and PFES volume fractions of 0.25 and 0.36 , respectively, were investigated. Both materials adopted cylindrical morphologies in the bulk. Emphasis was placed on the determination of the morphology of thin film specimens solvent annealed using toluene. Thin films were prepared by spin as well as dip-coating. As cast thin films of both materials prepared by spin-coating (100 nm thick) resulted in a disordered cylindrical morphology. Annealing the films in a saturated toluene vapor atmosphere yielded films with a highly ordered hexagonal lattice oriented normal to the surface. The high concentration of toluene mediated the film–air interfacial interactions sufficiently to obtain a perpendicular orientation. SAXS and scanning force microscopy (SFM) were used to determine a periodicity of approximately 42 nm. Dip-coating was used to prepare films less than 15 nm in thickness. These ultra thin films produced “very well-ordered” hexagonal arrays normal to the surface. However, TEM analysis showed that there was a well defined feature, approximately 5 nm in diameter, at the center of each cylindrical microdomain. The exact composition of this feature was further investigated by subjecting the films to UV/ozonolysis, which selectively degraded the PS block, leaving a PFES-based nanostructured inorganic oxide moiety. Close inspection of these nanostructures by TEM revealed that there was a pore running down the center of each cylinder, indicating that an inorganic oxide ring had been formed. The authors suggest that during solvent evaporation “an enlarged copolymer morphology is frozen in as the glass-transition temperature of the PS is traversed and further evaporation of the solvent opens a hole in the center of the cylindrical microdomain.” These nanoring structures are desirable for applications such as magnetic data storage. Their fabrication has been historically challenging, but this block copolymer methodology gives a facile route to such structures.

Several examples of the fabrication of nanostructured inorganic films have also been described. Malenfant and Wan et al. reported the preparation of nano-ordered ceramic materials.⁶⁸ The materials were prepared from a novel block copolymer synthesized by the ring opening metathesis polymerization of norbornene and a norbornene derivative with a pendent decaborane moiety. The total number-average molecular weight of the polymer was 61.0 kg mol^{-1} and it was composed of 30 mol% of the decaborane moiety.

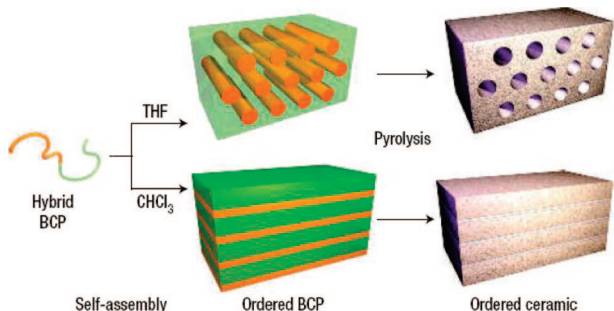


Figure 18. Preparation of ordered ceramic structures from polynorbornene diblock materials. Reprinted with permission from ref 68. Copyright 2007 Macmillan Publishers.

Macroscopic films of the material were prepared from THF and chloroform, with the morphological behavior changing depending on the solvent (Figure 18). Films cast from THF formed a cylindrical morphology, whereas a lamellar morphology resulted when chloroform was used. The authors claimed preferential solvation of the polynorbornene-decaborane block by THF to explain these morphological changes. After thermal annealing at 100 °C for 24 h, the samples were pyrolyzed in an ammonia atmosphere at 400 °C for 1 h and subsequently at 1000 °C for 4 h. This example is a nice demonstration of the fabrication of lamellar and cylindrical inorganic monoliths directly from block copolymer precursors. These types of methods could prove to have significant utility.

Finally, Ho et al. recently reported the successful production of nanoporous carbon materials from poly(acrylonitrile)-*b*-poly(ϵ -caprolactone) (PAN-PCL) block copolymers.⁶⁹ PAN-PCL materials were synthesized by sequential ring-opening polymerization/ATRP methods, with samples that demonstrated a lamellar morphology being the target for this study. Solution cast films of the PAN-PCL materials were heated to 230 °C for 20 h in an air atmosphere to “stabilize” the PAN structures (the nitrile side groups polymerize to form a cross-linked network), followed by heating at 800 °C under a vacuum to simultaneously thermally degrade the PCL and carbonize the PAN. Mesoporous carbon structures were evident by SEM. Chemical degradation of the PCL block using NaOH or KOH was also investigated, but the nitrile groups of the PAN block were also hydrolyzed. These techniques can potentially lead to a promising and convenient method for manufacturing mesoporous carbon sheets.

5. Membranes and Thin Films

In 2006, Joo et al. used PS-PMMA thin films as precursors to nanoporous coatings for antireflection applications.⁷⁰ Appropriate tuning of thin film refractive index can lead to antireflection properties. In most cases, porosity in the thin film coating is needed to achieve the targeted low refractive index. Spin coating a PS-PMMA block copolymer with 69% PMMA from toluene onto a glass substrate gave a disorganized morphology that was kinetically trapped because of rapid solvent evaporation. Nonetheless, upon exposure to UV radiation and an acetic acid rinse, a “spongelike” nanoporous PS structure was generated. The predicted reflectances,

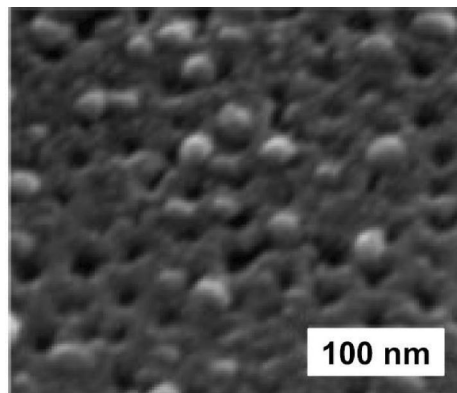


Figure 19. SEM image of a nanoporous membrane derived from an ordered block copolymer with excluded human rhinovirus 14 viroids on the surface. Reprinted with permission from ref 71. Copyright 2006 Wiley-VCH Verlag GmbH & Co. KGaA.

considering the refractive indices of PS, air, and glass, the thickness of the film, and the incident wavelength, were in very good agreement with the measured values. In fact, simple predictions of the film refractive index were consistent with the level of porosity anticipated by the volume fraction of PMMA in the block copolymer. Using the same protocol with PS-PMMA block copolymers containing different amounts of PMMA led to larger values of the minimum reflectance. This is a nice example of using block copolymers to template porous thin films without special alignment or surface modification methods. In the case of antireflective films, long-range order is not required and thus the disordered spongelike structure is quite effective.

Nanoporous membranes generated from ordered block copolymers have also been explored for separation applications and several recent papers have appeared that show promising results in this arena. Yang et al. prepared a blend of a PS-PMMA block copolymer and a PMMA homopolymer and then deposited it on a silicon wafer that had been treated with a random PS-PMMA copolymer.⁷¹ Perpendicular orientation of the cylindrical microdomains was observed in a thin film that was about 80 nm thick. This film was floated off of the underlying silicon substrate using HF, deposited on a supporting (large pore size) polysulfone membrane, and then treated with acetic acid to remove the PMMA homopolymer and generate nanopores about 15 nm in diameter. This supported membrane assembly was then evaluated in the filtration of viruses from an aqueous dispersion. The authors compared the separation efficiency of the block copolymer derived membrane with a commercially available track-etch polycarbonate membrane with similar pore size. Both separation membranes were extremely effective at removing human rhinovirus type 14 as evidenced by a sensitive plaque assay. An SEM image showing the virus particles on the block copolymer derived membrane is shown in Figure 19. Importantly, the flux of solution through the block-copolymer-derived membrane was more than 100 times higher than the polycarbonate membrane. This increase in flux was attributed to a combination of smaller film thickness and larger pore fraction in the block-copolymer-derived membrane. This work is a very good example that demonstrates the utility of block copolymer membranes for

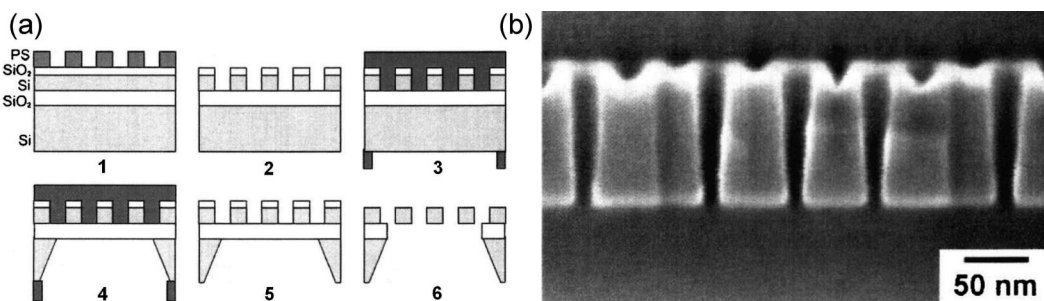


Figure 20. Nanoporous silicon membranes: (a) schematic process for membrane fabrication and (b) SEM image of 100 nm thick membrane. Reprinted with permission from ref 74. Copyright 2006 American Institute of Physics.

advanced separation applications that could have practical utility in water purification and biomedical applications.

In 2006, two papers describing gas and liquid transport through nanoporous plastics templated from block copolymers appeared. Cooney et al.⁷² and Phillip et al.⁷³ prepared nanoporous membrane assemblies from shear-aligned pieces of cylinder forming diblock copolymers or triblock terpolymers. Cooney et al. used a liquid diffusion cell to measure the diffusion constant for an aqueous NaOH solution through a 2 mm piece of a nanoporous membrane prepared by the etching of a PS-PLA block copolymer. Diffusion constants for NaOH were determined using either the measured breakthrough time, or the steady-state diffusivity based on the flux of hydroxide ions through the membrane. Since poor wetting of the membrane in pure aqueous solutions was a source of inconsistency between the two diffusion measurements, the two measured diffusion coefficients were about a factor of 10 different. The breakthrough diffusion coefficient was smaller than predicted (possibly due to interactions of the diffusing species with functionality remaining on the pore walls), and about an order of magnitude greater than the diffusivity based on the flux measurement. The discrepancy between the flux measurement and the breakthrough measurement was explained by imperfections in the pore structure; tortuosity and other pore defects were not accounted for in the diffusion model. Nonetheless, this work demonstrated that membrane assemblies from etched block copolymers behave essentially as expected, given the pore geometry, porosity, and pore alignment.

Using a very similar membrane assembly from an etched PS-PDMA-PLA triblock terpolymer,⁴⁵ Phillip et al. performed complementary transport measurements in both gas and liquid cells.⁷³ In the gas diffusion experiments, the linear plots of the natural log of the ratio of the pressure differences between the donating and receiving reservoirs with time were observed for He, Ar, N₂, and O₂. From the slopes of these plots, the permeability and thus the diffusion coefficient (accounting for the void fraction of the membrane and the tortuosity) could be calculated. The experimental diffusion coefficients for the four gases through these membranes were in quantitative agreement with predicted values based on a Knudsen diffusion mechanism, a pore fraction of 0.26, and a pore diameter of about 14 nm. In addition, liquid water flow through the same membranes gave fluxes consistent with pores of about 13 nm in diameter (in excellent agreement with the gas diffusion experiments). The pore diameters calculated from these macroscopic measurements

were not in quantitative agreement with the microscopically measured pore diameters using SEM or inferred from SAXS. Both methods gave pore diameters of about 17 nm. This discrepancy could be the result of nonideal pore geometry details of the pore wall chemistry. Although quantitative agreement between the microscopic and macroscopic measurements was not realized, the results of this study certainly verified the promising potential of block-copolymer-based membranes in ultrafiltration applications. In fact, the authors included a comparative analysis of idealized block copolymer based membranes and commercially available membranes for the separation of bovine serum albumin. Block copolymer membranes like the ones described in this report could simultaneously exhibit dramatically enhanced permeabilities and selectivities. The authors stated “We look forward to finding out if this expected improvement can be achieved experimentally for aqueous ultrafiltration.”

A set of nanoporous silicon membranes templated by PS-PMMA block copolymers were reported by Black et al. in 2006.⁷⁴ Using a pattern transfer process and a “silicon-on-insulator” substrate, the authors were able to etch through a nanoporous polystyrene thin film to the silicon or silicon oxide layers using RIE processes. After coating with silicon nitride and patterning the backside of the wafer, using traditional photolithography, they were able to ultimately generate a suspended nanoporous film of silicon that was about 100 nm thick. A schematic of the overall process and a cross-section of the film are shown in Figure 20. Using various established techniques for changing the pore size of the PS template, the authors suggested that this process can be useful for generating silicon membranes with a range of pore sizes. However, they did warn that optimizing all the processing steps can be somewhat difficult. In an alternative approach to changing the pore size of their silicon membranes, the authors described a few postprocessing techniques that are used in the semiconductor industry. These include thermal oxidation and atomic layer deposition methods, which could be used to both enlarge and shrink the pores. This work demonstrates how nanoporosity in thin polymer films from ordered block copolymers can be transferred to other materials that could be potentially useful for nanoporous membrane applications, such as molecular separations.

6. Summary and Perspective

Recent advances in block copolymer science and technology have enabled the formation of a wide variety of

nанопорозных материалов, что дает много обещаний в quite a diverse array of advanced applications. By using block copolymers that contain at least one sacrificial (etchable) block, many researchers have built on Nakahama's original discovery 20 years ago⁴ and have shown that much is possible using this concept. The principal area of research using nanoporous polymers derived from ordered block copolymers has been in the area of nanolithography. Both as lithographic templates for selective deposition of materials, or as templates for pattern transfer, nanoporous polymers have been shown to be quite useful. There is no question that future advances are yet to come. Although new processing parameters and protocols will enable novel applications in this area, new block copolymer chemistries will be centrally important in facilitating future progress in the field. Mild etch techniques, spontaneous alignment, etch resistance, specific chemical functionality, etc., can all be controlled in principle by utilizing particular chemical repeating units incorporated into block copolymers. So, as new combinations of polymer segments are stitched together using controlled polymerization methods, novel applications in the area of nanoporous templates for lithographic applications will emerge. Also important to the development of this field, is the ability to have extremely long-range order in the templates. The directed assembly techniques described have certainly been important advances in this regard.

Two other application areas that are most promising for nanoporous materials derived from ordered block copolymers are in membrane separations and catalyst-supports. Free-standing materials (i.e., films or monoliths not supported on other substrates) will be important to develop for both of these applications. For the next level of accomplishment in this area, mechanically robust materials and materials with specifically functionalized pore walls will need to be further developed. Important advances have been made using, for example, semicrystalline matrices for mechanical strength⁵⁷ and etchable ABC triblocks as precursors to nanoporous polymers with specific pore wall coatings.^{44–46} Nanoporous membranes derived from block copolymers have the potential to be extremely effective as separation membranes given their very narrow pore size distributions and high porosities. We see efforts at developing robust and inexpensive technologies for this purpose as important future research endeavors. Using related materials as supports for catalysts will also be interesting to develop, given precedents in inorganic mesoporous materials. Selective membrane reactors and biocatalysis applications are areas that may be particularly well suited for nanoporous materials from block copolymers.

Block copolymers have and will continue to fascinate scientists as self-assembling materials with nanoscopic features. There are obviously many ways to exploit these attributes in applications; however, the formation of porosity has captured the imagination of many researchers. Nanoporous materials prepared from ordered block copolymer templates have come a long way in the past two decades, and exciting future advances in this field are yet to come.

Acknowledgment. Thank you to Adam J. Meuler for a thorough and detailed review of this manuscript prior to

submission. Work in the Hillmyer Research Group at the University of Minnesota in the area of nanoporous materials has been funded over the past several years by the National Science Foundation, the David and Lucile Packard Foundation, the Camille and Henry Dreyfus Foundation, and the Department of Energy. We are grateful for their support.

References

- (1) (a) Hamley, I. W. *The Physics of Block Copolymers*; Oxford University Press: Oxford, U.K., 1998. (b) Hadjichristidis, N.; Pispas, S.; Floudas, G. A. *Block Copolymers: Synthetic Strategies, Physical Properties, and Applications*; Wiley-Interscience: New York, 2003.
- (2) (a) Lodge, T. P. *Macromol. Chem. Phys.* **2003**, *204*, 265–273. (b) Bates, F. S.; Fredrickson, G. H. *Phys. Today* **1999**, *52*, 32–38. (c) Hamley, I. W. *Angew. Chem., Int. Ed.* **2003**, *42*, 1692–1712. (d) Park, C.; Yoon, J.; Thomas, E. L. *Polymer* **2003**, *44*, 6725–6760.
- (3) (a) Fredrickson, G. H.; Bates, F. S. *Annu. Rev. Mater. Sci.* **1996**, *26*, 501–550. (b) Hamley, I. W. *J. Phys.: Condens. Matter* **2001**, *13*, R643–R671.
- (4) Lee, J.-S.; Hirao, A.; Nakahama, S. *Macromolecules* **1988**, *21*, 274–276.
- (5) Hillmyer, M. A. *Adv. Polym. Sci.* **2005**, *190*, 137–181.
- (6) Park, M.; Harrison, C.; Chaikin, P. M.; Register, R. A.; Adamson, D. H. *Science* **1997**, *276*, 1401–1404.
- (7) Zalusky, A. S.; Olayo-Valles, R.; Taylor, C. J.; Hillmyer, M. A. *J. Am. Chem. Soc.* **2001**, *123*, 1519–1520.
- (8) Hawker, C. J.; Russell, T. P. *MRS Bull.* **2005**, *30*, 952–966.
- (9) Service, R. F. *Science* **2006**, *314*, 1868–1870.
- (10) Hamm, S. IBM's Chip Breakthrough. *Business Week* [Online] May 3, **2007**.
- (11) Thurn-Albrecht, T.; Steiner, R.; DeRouche, J.; Stafford, C. M.; Huang, E.; Bai, M.; Tuominen, M.; Hawker, C. J.; Russell, T. P. *Adv. Mater.* **2000**, *12*, 787–791.
- (12) Melde, B. J.; Burkett, S. L.; Xu, T.; Goldbach, J. T.; Russell, T. P.; Hawker, C. J. *Chem. Mater.* **2005**, *17*, 4743–4749.
- (13) Zschech, D.; Kim, D. H.; Milenin, A. P.; Hopfe, S.; Scholz, R.; Göring, P.; Hillebrand, R.; Senz, S.; Hawker, C. J.; Russell, T. P.; Steinhart, M.; Gösele, U. *Nanotechnology* **2006**, *17*, 2122–2126.
- (14) Zschech, D.; Kim, D. H.; Milenin, A. P.; Scholz, R.; Hillebrand, R.; Hawker, C. J.; Russell, T. P.; Steinhart, M.; Gösele, U. *Nano Lett.* **2007**, *7*, 1516–1520.
- (15) Hozumi, A.; Asakura, S.; Fuwa, A.; Shirahata, N. *J. Colloid Interface Sci.* **2005**, *285*, 875–878.
- (16) Asakura, S.; Hozumi, A.; Fuwa, A. *J. Vac. Sci. Technol., A* **2005**, *23*, 1137–1140.
- (17) Zhang, Q.; Xu, T.; Butterfield, D.; Misner, M. J.; Ryu, D. Y.; Emrick, T.; Russell, T. P. *Nano Lett.* **2005**, *5*, 357–361.
- (18) Zhang, Q.; Gupta, S.; Emrick, T.; Russell, T. P. *J. Am. Chem. Soc.* **2006**, *128*, 3898–3899.
- (19) Darling, S. B.; Yu, N. A.; Cisse, A. L.; Bader, S. D.; Sibener, S. J. *Adv. Mater.* **2005**, *17*, 2446–2450.
- (20) Bandyopadhyay, K.; Tan, E.; Ho, L.; Bundick, S.; Baker, S. M.; Niemz, A. *Langmuir* **2006**, *22*, 4978–4984.
- (21) Fu, G.-D.; Yuan, Z.; Kang, E.-T.; Neoh, K.-G.; Lai, D. M.; Huan, A. C. H. *Adv. Funct. Mater.* **2005**, *15*, 315–322.
- (22) Hedrick, J. L.; Carter, K. R.; Labadie, J. W.; Miller, R. D.; Volksen, W.; Hawker, C. J.; Yoon, D. Y.; Russell, T. P.; McGrath, J. E.; Briber, R. M. *Adv. Polym. Sci.* **1999**, *141*, 1–43.
- (23) Chung, C.-M.; Lee, J.-H.; Cho, S.-Y.; Kim, J.-G.; Moon, S.-Y. *J. Appl. Polym. Sci.* **2006**, *101*, 532–538.
- (24) Lu, S.-Y.; Chang, C.-H.; Yu, C.-H.; Chen, H.-L.; Lo, Y. H. *J. Mater. Res.* **2005**, *20*, 1523–1528.
- (25) Olayo-Valles, R.; Guo, S.; Lund, M. S.; Leighton, C.; Hillmyer, M. A. *Macromolecules* **2005**, *38*, 10101–10108.
- (26) Fasolka, M. J.; Mayes, A. M. *Annu. Rev. Mater. Res.* **2001**, *31*, 323–355.
- (27) Johnson, B. J. S.; Wolf, J. H.; Zalusky, A. S.; Hillmyer, M. A. *Chem. Mater.* **2004**, *16*, 2909–2917.
- (28) Lo, K.-H.; Tseng, W.-H.; Ho, R.-M. *Macromolecules* **2007**, *40*, 2621–2624.
- (29) Crossland, E. J. W.; Ludwigs, S.; Hillmyer, M. A.; Steiner, U. *Soft Matter* **2007**, *3*, 94–98.
- (30) Guo, S.; Rzayev, J.; Bailey, T. S.; Zalusky, A. S.; Olayo-Valles, R.; Hillmyer, M. A. *Chem. Mater.* **2006**, *18*, 1719–1721.
- (31) Bang, J.; Kim, S. H.; Drockenmuller, E.; Misner, M. J.; Russell, T. P.; Hawker, C. J. *J. Am. Chem. Soc.* **2006**, *128*, 7622–7629.
- (32) Ryu, D. Y.; Shin, K.; Drockenmuller, E.; Hawker, C. J.; Russell, T. P. *Science* **2005**, *308*, 236–239.
- (33) Niemz, A.; Bandyopadhyay, K.; Tan, E.; Cha, K.; Baker, S. M. *Langmuir* **2006**, *22*, 11092–11096.
- (34) Stoykovich, M. P.; Müller, M.; Kim, S. O.; Solak, H. H.; Edwards, E. W.; de Pablo, J. J.; Nealey, P. F. *Science* **2005**, *308*, 1442–1446.
- (35) Park, S.-M.; Craig, G. S. W.; La, Y.-H.; Solak, H. H.; Nealey, P. F. *Macromolecules* **2007**, *40*, 5084–5094.
- (36) Stoykovich, M. P.; Park, S.-M.; Papakonstantopoulos, Y. J.; de Pablo, J. J.; Nealey, P. F.; Solak, H. H. *Phys. Rev. Lett.* **2006**, *96*, 031604.
- (37) Li, H.-W.; Huck, W. T. S. *Nano Lett.* **2004**, *4*, 1633–1636.
- (38) Xiao, S.; Yang, X.; Edwards, E. W.; La, Y.-H.; Nealey, P. F. *Nanotechnology* **2005**, *16*, S324–S329.

- (39) Kim, S. H.; Misner, M. J.; Yang, L.; Gang, O.; Ocko, B. M.; Russell, T. P. *Macromolecules* **2006**, *39*, 8473–8479.
- (40) Li, X.; Zhao, S.; Zhang, S.; Kim, D. H.; Knoll, W. *Langmuir* **2007**, *23*, 6883–6888.
- (41) Melosh, N. A.; Davidson, P.; Chmelka, B. F. *J. Am. Chem. Soc.* **2000**, *122*, 823–829.
- (42) Svec, F. *J. Sep. Sci.* **2005**, *28*, 729–745.
- (43) Boger, T.; Heibel, A. K.; Sorensen, C. M. *Ind. Eng. Chem. Res.* **2004**, *43*, 4602–4611.
- (44) Rzayev, J.; Hillmyer, M. A. *Macromolecules* **2005**, *38*, 3–5.
- (45) Rzayev, J.; Hillmyer, M. A. *J. Am. Chem. Soc.* **2005**, *127*, 13373–13379.
- (46) Bailey, T. S.; Rzayev, J.; Hillmyer, M. A. *Macromolecules* **2006**, *39*, 8772–8781.
- (47) Mao, H.; Hillmyer, M. A. *Macromolecules* **2005**, *38*, 4038–4039.
- (48) Mao, H.; Hillmyer, M. A. *Soft Matter* **2006**, *2*, 57–59.
- (49) Okumura, A.; Nishikawa, Y.; Hashimoto, T. *Polymer* **2006**, *47*, 7805–7812.
- (50) Hashimoto, T.; Nishikawa, Y.; Tsutsumi, K. *Macromolecules* **2007**, *40*, 1066–1072.
- (51) Zhou, N.; Bates, F. S.; Lodge, T. P. *Nano Lett.* **2006**, *6*, 2354–2357.
- (52) Hillmyer, M. A.; Maurer, W. W.; Lodge, T. P.; Bates, F. S.; Almdal, K. J. *Phys. Chem. B* **1999**, *103*, 4814–4824.
- (53) Ha, J.-M.; Hillmyer, M. A.; Ward, M. D. *J. Phys. Chem. B* **2005**, *109*, 1392–1399.
- (54) Drockenmuller, E.; Li, L. Y. T.; Ryu, D.-Y.; Harth, E.; Russell, T. P.; Kim, H.-C.; Hawker, C. J. *J. Polym. Sci., Part A: Polym. Chem.* **2005**, *43*, 1028–1037.
- (55) Leiston-Belanger, J. M.; Russell, T. P.; Drockenmuller, E.; Hawker, C. J. *Macromolecules* **2005**, *38*, 7676–7683.
- (56) Guo, F.; Andreasen, J. W.; Vigild, M. E.; Ndoni, S. *Macromolecules* **2007**, *40*, 3669–3675.
- (57) Uehara, H.; Yoshida, T.; Kakiage, M.; Yamanobe, T.; Komoto, T.; Nomura, K.; Nakajima, K.; Matsuda, M. *Macromolecules* **2006**, *39*, 3971–3974.
- (58) Yokoyama, H.; Li, L.; Nemoto, T.; Sugiyama, K. *Adv. Mater.* **2004**, *16*, 1542–1546.
- (59) Li, L.; Yokoyama, H.; Nemoto, T.; Sugiyama, K. *Adv. Mater.* **2004**, *16*, 1226–1229.
- (60) Yokoyama, H.; Sugiyama, K. *Macromolecules* **2005**, *38*, 10516–10522.
- (61) Li, L.; Nemoto, T.; Sugiyama, K.; Yokoyama, H. *Macromolecules* **2006**, *39*, 4746–4755.
- (62) Laforge, A.; Bazuin, C. G.; Prud'homme, R. E. *Macromolecules* **2006**, *39*, 6473–6482.
- (63) Fustin, C. A.; Lohmeijer, B. G. G.; Duwez, A.-S.; Jonas, A. M.; Schubert, U. S.; Gohy, J.-F. *Adv. Mater.* **2005**, *17*, 1162–1165.
- (64) Zhang, M.; Yang, L.; Yurt, S.; Misner, M. J.; Chen, J.-T.; Coughlin, E. B.; Venkataraman, D.; Russell, T. P. *Adv. Mater.* **2007**, *19*, 1571–1576.
- (65) Li, L.; Yokoyama, H. *Angew. Chem., Int. Ed.* **2006**, *45*, 6338–6341.
- (66) Rider, D. A.; Cavicchi, K. A.; Vanderark, L.; Russell, T. P.; Manners, I. *Macromolecules* **2007**, *40*, 3790–3796.
- (67) Rider, D. A.; Cavicchi, K. A.; Power-Billard, K. N.; Russell, T. P.; Manners, I. *Macromolecules* **2005**, *38*, 6931–6938.
- (68) Malenfant, P. R. L.; Wan, J.; Taylor, S. T.; Manoharan, M. *Nat. Nanotechnol.* **2007**, *2*, 43–46.
- (69) Ho, R.-M.; Wang, T.-C.; Lin, C.-C.; Yu, T.-L. *Macromolecules* **2007**, *40*, 2814–2821.
- (70) Joo, W.; Park, M. S.; Kim, J. K. *Langmuir* **2006**, *22*, 7960–7963.
- (71) Yang, S. Y.; Ryu, I.; Kim, H. Y.; Kim, J. K.; Jang, S. K.; Russell, T. P. *Adv. Mater.* **2006**, *18*, 709–712.
- (72) Cooney, D. T.; Hillmyer, M. A.; Cussler, E. L.; Moggridge, G. D. *Crystallogr. Rev.* **2006**, *12*, 13–24.
- (73) Phillip, W. A.; Rzayev, J.; Hillmyer, M. A.; Cussler, E. L. *J. Membr. Sci.* **2006**, *286*, 144–152.
- (74) Black, C. T.; Guarini, K. W.; Breyta, G.; Colburn, M. C.; Ruiz, R.; Sandstrom, R. L.; Sikorski, E. M.; Zhang, Y. *J. Vac. Sci. Technol., B* **2006**, *24*, 3188–3191.

CM702239K